Qualitative and quantitative approach towards the molecular understanding of structural, vibrational and optical features of Urea ninhydrin monohydrate

Sasikala V.[a], D. Sajan[a*], K. Chaitanya[b], Tom Sundius[c], T. Uma Devi[d]

[a]*Department of Physics, Bishop Moore College, Mavelikara, Alappuzha, Kerala-690110, India.*

[b]*Department of Chemistry, Nanjing University of Science and Technology, Xialingwei 200, Nanjing, People's Republic of China.*

[c]*Department of Physics, University of Helsinki, Finland.*

[d]*Department of Physics, Government Arts College for Women (Autonomous), Pudukottai, India.*

*Corresponding author:Dr. D. Sajan

E-mail addresses: drsajanbmc@gmail.com, dsajanbmc@gmail.com

Tel: +91-9495043765, Fax: +91-479 2303230

ABSTRACT

In this study, single crystals of urea ninhydrin monohydrate (UNMH) have been grown by slow evaporation method. The grown crystals were characterized by FT-IR, FT-Raman and UV-Vis-NIR spectroscopies. The Kurtz and Perry powder method was employed to confirm the near-zero SHG efficiency of the as-grown centrosymmetric UNMH crystal. The third order nonlinearity of the crystal has been studied by the open aperture Z-scan method. The nonlinear absorption coefficient is calculated and the potentiality of UNMH in optical limiting applications is identified. The molecular geometry and the origin of optical non-linearity at the molecular level have been investigated by the density functional theory. The normal coordinate analysis was carried out to assign the molecular vibrational modes. Vibrational spectral studies confirms the presence of weak O-H···O and moderate O-H···O type hydrogen bonds in the molecule as well as O-H···O, N-H···O and blue-shifted C-H···O type H-bonds in the crystal. The intramolecular charge transfer interactions and the electronic absorption mechanisms have been discussed. The static and the dynamic values of hyperpolarizabilities for UNMH were estimated theoretically by DFT methods.

Keywords: NBO; Z-scan; hyperpolarizability; cubic nonlinearity; vibrational spectra.

1. Introduction

The overall non-linear optical (NLO) activity of a crystalline material in an electric field depends on its molecular structure, presence of molecular chromophores, inter and intra molecular electron transfer mechanism, molecular association and correlation, magnitudes of molecular hyperpolarizability tensor components, nature of the relevant crystal point group and the degree of molecular orientation within the crystalline reference frame [1,2]. The subtle variations in molecular architecture [1, 3-5] such as size, shape, symmetry; geometry etc. can lead to drastic changes in the NLO response properties of molecular crystals. Organic molecules that crystallize in a non-centrosymmetric space group display the second-order NLO property whereas in the case of centrosymmetric crystalline system, the influence of molecular orientations in the crystalline unit cell cancels out the nonlinear efficiencies of individually optimized molecular units, hence there is no second-order NLO activity [1, 6] but there are some exceptions also [7, 8]. The alteration of second order NLO property in the centrosymmetric system can be achieved through the modification of the crystal structure by the synergistic combinations of highly nonlinear molecules to its crystal structure which alters the molecular geometry and intramolecular charge transfer interactions, and hence the second order NLO activity [3].

The present study emphasizes on the qualitative and quantitative structure and NLO property relationships of an organic centrosymmetric crystal, urea ninhydrin monohydrate (UNMH) based on the molecular and electronic structural property elucidation using quantum chemical computations and experimental investigations. The crystal growth and characterization studies of urea ninhydrin monohydrate have been reported [9]. The crystal belongs to the centrosymmetric monoclinic space group [9], $P2_1/c$. The main constituents of UNMH are the known organic NLO materials, urea and ninhydrin and both of the components belong to the non-centrosymmetric crystalline system. Urea crystallizes in tetragonal-scalenohedral space group [10, 11], $P\bar{4}2_1m$ whereas ninhydrin has a monoclinic

lattice with $P2_1$ space group [12]. These organic molecular crystals are hydrogen bonded and have the capability to form long-range dipolar interactions and polarization effects within the system that promotes their noncentric lattices. Urea has been extensively studied as an organic NLO active benchmark system capable of efficient second harmonic generation because of its individual molecular properties which is influenced by the possibilities of hydrogen bonds formed between C=O and N-H bonds of the molecule and neighbouring urea molecules in the crystalline state. The crystalline urea has exceptionally high ultra-violet transparency up to 200 nm and it has large birefringence. Ninhydrin is a stable hydrated product of indane-1,2,3-trione, which is considered to be an important building block in organic synthesis. Ninhydrin has the capability to form complex heterocyclic compounds by multicomponent reactions which is accomplished through its more reactive C-2 site. This site of ninhydrin is positioned between two adjacent carbonyl groups where two hydroxyl groups are attached to the same carbon atom and this site is more reactive towards oxygen, sulphur and carbon based nucleophiles. A lot of studies have been previously published based on the structural [10-14], vibrational [15-21] and NLO properties [22-31] of urea and ninhydrin. Significant efforts have concentrated on investigating the molecular level mechanisms in such organic systems based on the appropriate electron donor-acceptor interactions and optical nonlinearity [32,33] by vibrational spectroscopy based on the density functional theory (DFT) quantum chemical computational method [34-36]. A systematical study using the experimental observations and the theoretical predictions on molecular structure, vibrational, electronic and nonlinear properties for the title crystal is necessary for the design of new and efficient NLO materials for photonics applications and to identify the potentiality of the title crystal in the relevant field of NLO applications.

In the present study, single crystals of UNMH have been grown and spectral characterizations are done using FT-IR, FT-Raman and UV-Vis-NIR techniques. The NLO behaviour of UNMH has been investigated using the Kurtz-Perry powder method and the open-aperture Z-scan method. The molecular level structural, vibrational, electronic and

4

nonlinear properties have been explored using the DFT/B3LYP/cc-pVTZ level of computation. The intramolecular interactions capable of inducing the NLO property to the molecule present in the structure and its polarizability (hyper) values have been discussed and compared with those values of the similar organic molecular system.

2. Material and methods

2.1 Experimental methods

2.1.1 Sample preparation

An aqueous solution of UNMH was prepared from the equimolar amount (1:1 stoichiometric ratio) of urea and ninhydrin in double distilled water. The solubility of UNMH in water was determined gravimetrically as a function of temperature in the range 35-55 °C. The resulting solubility curve is shown in Fig. 1(a). The results indicate that the solubility temperature coefficient of UNMH has a large positive value which is indicating its excellent solubility in water.

- **Figure 1**

A saturated solution of urea and ninhydrin in distilled water was prepared in accordance with the solubility data. The single crystals of UNMH were grown by slow evaporation of solution technique at the room temperature (30°C). Optically transparent single crystals were obtained after a period of 10 days. The purity of the crystal was improved by repeated recrystallization process. The photograph of as-grown single crystals of UNMH is shown in Fig. 1(b).

2.1.2 Instrumentation

The FT-IR spectrum of the sample was recorded on JASCO FT/IR-4100 spectrometer in the range 4000-400 cm^{-1}. A Bruker RFS 100/S FT-Raman spectrometer was used to record the Raman spectrum in the range 4000-100 cm^{-1}. The UV-Vis-NIR absorption spectrum of UNMH was recorded in the range 190-1100 nm using a Shimadzu Model 1601

spectrophotometer. Kurtz and Perry powder method [22] was employed for the second harmonic generation efficiency measurement. For the SHG measurement, the sample was irradiated with laser pulses from a Q-switched Nd-YAG laser source of fundamental wavelength of 1064 nm with a pulse width of 10 ns and at a repetition rate of 10 Hz. The input beam energy of the laser was 1.2 mJ/pulse. Finally, the third order NLO property of the sample was studied using open aperture Z-scan technique [37] with 5 ns laser pulses at an excitation wavelength of 532 nm.

2.2 Computational methods

The optimization of the isolated gas-phase molecular structure and all other molecular level calculations were done at the DFT/B3LYP/cc-pVTZ level of theory [38-41] with the aid of the Gaussian 09W program package [42]. The calculated structure was visualized using the GaussView 5.0 program [43]. The structure stabilizing intramolecular charge transfer interactions in UNMH were analyzed using NBO 3.1 program [44] and the delocalization energies associated with the charge transfer interactions between bonding and antibonding orbitals were examined using the second order perturbation theory analysis of the Fock matrix in the NBO method.

The time dependent DFT (TDDFT) computation was performed to simulate the electronic absorption phenomena of gas and water phases for the molecule. The quantum mechanical force field calculated by Gaussian was scaled by multiple scaling factors using the MOLVIB program [45], and potential energy distributions and intensities of the normal modes were calculated for the optimized structure.

The static and dynamic values of first- and static- second electronic hyperpolarizabilities were calculated using the DFT/B3LYP method implemented in Gaussian 09W [46]. The frequency independent static first- hyperpolarizabilities were calculated for the molecule at both the 6-311++G(d, p) [47] and the cc-pVTZ [41] basis sets. The dynamic first-hyperpolarizabilities were evaluated theoretically with B3LYP/cc-pVTZ level at the

6

characteristic Nd:YAG laser wavelength, 1064 nm ($\hbar\omega$= 0.042823 au) for the second harmonic generation, $\beta(-2\omega; \omega, \omega)$ and the electro-optical Pockels effect, $\beta(-\omega; \omega, 0)$. The static second-hyperpolarizability was also calculated with the DFT/B3LYP/cc-pVTZ level of the theory.

3. Results and Discussion

3.1 Optimized Geometry

According to the XRD crystal structure data [9], the monoclinic crystalline unit of UNMH has four molecules per unit cell (Z=4) that are linked by intermolecular O-H⋯O type H-bonds. These bonds were formed either between the hydroxyl groups of the water molecule and that of the urea-ninhydrin ring or between the hydroxyl groups of the ring systems. The intramolecular H-bonding was absent in the molecule. But in the bulk crystalline packing, the crystal system is stabilized by the formation of intermolecular N-H⋯O and C-H⋯O type interactions in addition to the O-H⋯O bonds and certainly, those can enhance the centrosymmetric crystalline close-packing of UNMH.

The optimized geometry of the UNMH molecule and two different views together with the atom numbering scheme adopted for DFT/B3LYP calculation is presented in Fig.2. The optimized monomeric structure consists of a benzene ring fused with a five-membered dicyclic ring system and a water molecule. The five-membered ring system contains a cyclopentanone ring of ninhydrin and a ring of urea moiety fused together. This ring system has a half-chair conformation.

- **Figure 2**

The isolated gas-phase molecule of UNMH has three intramolecular H-bonds that are weak O_{16}-H_{22}⋯O_{14} bonds within the urea-ninhydrin ring and moderate O_{25}-H_{26}⋯O_{13} and O_{14}-H_{21}⋯O_{25} bonds formed between the ring system and the water moiety. The selected optimized geometric and hydrogen bond parameters obtained from the DFT computation and the available crystal structure information [9] are given in Table 1.

7

• **Table 1**

The CC and the CH bond distances of a regular hexagonally shaped benzene ring are 1.395 Å and 1.085 Å, respectively [48]. However, in the case of UNMH, the observed CH bonds are shorter than the predicted values, which indicate the participation of C-H bonds in H-bonding interactions in the crystalline state. The C-C bond lengths of the benzene ring are calculated to be in the range 1.384-1.400 Å. The expansion of N_8-C_9-N_{10} ($\approx$109°) and the contraction of N-C=O ($\approx$126°) angles of the ring substituted urea moiety were observed due to the simultaneous involvement of its atoms in intramolecular N-H···O and O-H···O bonding and these bonds at the urea moiety were predicted to be absent in the gas phase molecule. The hydrogen bonding interactions at the carbonyl and NH sites decrease the observed C-N bond lengths of the urea moiety slightly below the calculated value but intermediate between the bond distances of a typical single bond (1.47 Å) and a double bond (1.26 Å). The observed bond length values of C-C bonds in the benzene ring and N-C bonds in the urea sub-unit show the extent of conjugation in them. The π-conjugation at the urea-ring in the crystalline state was probably due to the intermolecular H-bonding at the carbonyl and NH groups simultaneously.

The carbonyl bond of the ring substituted urea moiety (1.209 Å) is contracted below the XRD value (1.236 Å), whereas that in the fused cyclopentanone ring is found to be expanded by 0.009 Å over the observed value. The π-conjugation of the carbonyl group of the central ring with the benzene ring relays more electron density to C_5=C_6 and thus there is an increment in the C_5=C_6 bond length in addition to the C_{12}=O_{13} double bond strength. Through this charge transfer the C_5-C_{12} bond gets shortened over the other bond, while C_{11}-C_{12} is attached to the C_{12}=O_{13} bond. The dihedral angles of $C_4C_5C_{12}C_{11}$ (-175.4°), $C_2C_1C_6C_7$ (179.0°) and $C_4C_5C_{12}O_{13}$ (3.9°) specify the co-planarity of the central fused five-membered ring with the benzene ring.

The two hydroxyl groups attached to the five membered ring systems act as H-bond donor and acceptor and form a weak H-bonding due to steric repulsive interactions. The torsional angle (12.4°) of the skeleton ($O_{14}C_{11}C_7O_{16}$) comprising the space between the hydroxyl groups and its deviation from the plane of ring systems will substantiate such interactions which can be correlated with the inhibition of conjugation in the central ring. The torsional plane of each of the two hydroxyl groups is opposite to the plane of the fused five-membered ring system. This is obvious from the dihedral angles of $H_{22}O_{16}C_7C_6$ (-143.4°), $H_{22}O_{16}C_7N_8$ (87.3°), $H_{21}O_{14}C_{11}C_{12}$ (-67.0°) and $H_{21}O_{14}C_{11}N_{10}$ (61.0°).

It can be seen from the Table 1 that the endocyclic bond angles of the five-membered ring systems have small angular deformations both in the computational and experimental results and this may be ascribed to the minimum energy ring straining interactions. The dihedral angle values 101.1° for $C_5C_{12}C_{11}N_{10}$, -125.5° for $C_{12}C_{11}N_{10}C_9$, 65.3° for $C_1C_6C_7N_8$ and 102.3° for $C_6C_7N_8C_9$ indicate that the plane of the five membered ring containing the urea moiety deviates from the plane of the benzene and the fused central ring. The weak O_{16}-$H_{22}\cdots O_{14}$ bonding and the intramolecular charge transfer interaction especially due to the presence of nitrogen atoms which supports the reduction of angle strain in the substituted urea-ring will thus enable the molecule to twist or bend easily.

The predicted H-O-H angle of the V-shaped water molecule is slightly shortened and the O-H bond lengths are unequal. The decrement in angle and the increment in bond length values of the water molecule originated from its simultaneous electron donation and H-bond acceptance with the ring system. The repulsive interactions between the lone pairs of oxygen atom of the water molecule bring the two OH bond pairs of electrons closer, thus there is a reduction in the HOH angle.

3.2 NBO analysis

9

The calculated result of the foremost charge transfer interactions in UNMH by NBO analysis is listed in Table ST1 (*Supporting Information*). The three structure stabilizing n→σ* type hydrogen bonding interactions, O_{25}-H_{26}···O_{13}, O_{14}-H_{21}···O_{25} and O_{16}-H_{22}···O_{14} were identified for the molecule with low hyperconjugative delocalization energies and the estimated values of the total H-bond strength of each of these interactions are 32.95 kJ/mol, 57.57 kJ/mol and 6.15 kJ/mol, respectively. The H-bond forming negative hyperconjugations significantly increase the electron densities of the σ*-antibonding orbitals of O-H bonds which lead to the elongation of respective antibonds and hence the associated red shift in stretching wavenumbers.

The strong lone pair electron donating ability of the oxygen (O_{13}, O_{14} and O_{16}) and the nitrogen (N_8 and N_{10}) atoms to the skeletal carbon atoms of the central ring increases the σ-overlap of the ring by the hyperconjugative interactions with the σ*(C-C) orbitals and weakens the C-C sigma bonds of the ring. The electron density on the O_{13} atom is transferred significantly to the σ*-antibonding orbitals of C_5-C_{12} and C_{11}-C_{12} bonds through the hyperconjugations with stabilization energies of 89.47 kJ/mol and 82.98 kJ/mol, respectively. The p-electron depletion at the O_{13} atom resulted in the concomitant strengthening of C_{12}=O_{13} and weakening of C_5-C_{12} and C_{11}-C_{12} bonds. The dominant overlap between the sigma orbitals of the C-C bonds of the central fused ring resulted in the strongest sigma bond formations, which may lead to generation of a low ring strain energy that stabilizes the central five membered C-C ring system by sigma conjugative interaction energies in the range 2.89-8.42 kJ/mol.

NBO analysis identified two remote structure stabilizing lone pair delocalization interactions such as the hyperconjugative and the through-space charge transfer interactions due to nitrogen atoms of urea moiety. The former enhances the charge delocalization of π-aromatic cloud of the benzene ring by the distant-mesomeric effect due to the interactions between the lone pairs of N_8 atom and π-antibonding orbital of inter-ring bond, C_5-C_6. This

assists in balancing the close contact (2.498 Å-3.446 Å) of a heteroatom of the urea moiety to the benzene ring by providing a stabilization energy of 5.32 kJ/mol. The latter is due to the lone pairs of N_{10} atom and π^* orbital of C_{12}-O_{13} which facilitates the electron transport from the nitrogen atom to the carbonyl bond of the fused cyclopentanone ring through the short contact (2.445 Å-3.125 Å) and stabilizes the system by 9.76 kJ/mol. These n→π^* interactions facilitate the bending of the plane of urea moiety ring from the plane of benzene fused central ring and give an additional stabilization to the structure. The enormous π electron densities on the nitrogen atoms induce slightly the *s* but significantly the *p* characters to the carbonyl bond of urea moiety by imparting more charge density into the σ^* and π^* orbitals of C_9=O_{15} bond simultaneously with the stabilizing interactions of $n_1(N_8)$→$\sigma^*(C_9$-$O_{15})$/$\pi^*(C_9$-$O_{15})$ and $n(N_{10})$→$\sigma^*(C_9$-$O_{15})$/$\pi^*(C_9$-$O_{15})$ with high charge delocalization energies.

The $\sigma(O_{25}$-$H_{26})$ bonding orbitals of the water molecule interact with the ring system other than hydrogen bonding by σ-conjugation with very low delocalization energies. The stabilization energy associated with the anti-bonding orbitals of the five-membered ring bonds due to the inter-ring charge delocalization of the lone pairs of nitrogen and oxygen atoms were theoretically estimated to be in the range 22.06-55.14 kJ/mol. The two strong and co-operative structure stabilizing π-conjugations due to the carbonyl bond of the fused cyclopentanone ring and the benzene ring fusion bond, C_5-C_6 with stabilization energies of 113.33 kJ/mol and 16.29 kJ/mol were identified for the molecule.

The charge delocalizing effects to the $\sigma^*(C_9$-$N_{10})$ bond dominate over the other delocalization effects on the $\sigma^*(N_8$-$C_9)$ bond, resulting in a large single bond character of the C_9-N_{10} bond compared to that of the N_8-C_9 bond. The charge transfer interactions directed from the lone pairs of oxygen atom (O_{15}) to the $\sigma^*(N_8$-$C_9)$ and the $\sigma^*(C_9$-$N_{10})$ antibonding NBO orbitals confirm the resonance effect in urea moiety.

The benzene ring is stabilized by the π-electron delocalization through energetic $\pi(CC)$→$\pi^*(CC)$ interactions and by the σ-electron delocalization through the cyclic and co-

operative sigma conjugation of $\sigma(C_1-C_2)\leftrightarrow\sigma(C_2-C_3)$, $\sigma(C_2-C_3)\leftrightarrow\sigma(C_3-C_4)$, $\sigma(C_3-C_4)\leftrightarrow\sigma(C_4-C_5)$, $\sigma(C_4-C_5)\leftrightarrow\sigma(C_5-C_6)$, $\sigma(C_5-C_6)\leftrightarrow\sigma(C_1-C_6)$ and $\sigma(C_1-C_6)\leftrightarrow\sigma(C_1-C_2)$ with second order delocalization energies in the range 70.21-100.61 kJ/mol and 6.78-16.24 kJ/mol, respectively. The hyperconjugative interactions between the σ-electrons of C-H bonds and skeletal CC bonds of the benzene ring cause the charge delocalization into the antibonding σ-system and induce greater stability to the ring by giving a second order estimate in the range 2.81-22.11 kJ/mol for $\sigma(CH)\rightarrow\sigma^*(CC)$, 3.01-13.10 kJ/mol for $\sigma(CC)\rightarrow\sigma^*(CH)$ and 2.14-2.55 kJ/mol for mutual and adjacent sigma bond orbital overlapping of CH bonds. The π and σ bonding systems of the benzene ring moiety constitute significant resonance stabilization to the molecule.

The natural population analysis results are listed in Table ST2 (*Supporting Information*) giving the atomic natural charge on each atom. The oxygen (O_{25}) atom of water molecule has the maximum negative charge (-0.9629e) and the carbonyl carbon atoms of the fused urea-ring moiety and the central fused cyclopentanone rings have the highest (0.7799e) and the second highest (0.5596e) positive charges, respectively. The highest negative charge on the oxygen atom of water molecule reveals its enhanced electron donating ability. The formation of $O_{25}-H_{26}\cdots O_{14}$ and $O_{25}-H_{26}\cdots O_{13}$ bonds, and the absence of geminal interactions also constitute a high negative charge to the oxygen atom of water molecule. The carbonyl group of urea moiety enhances the stabilization of the ring by strong π-electron delocalization by putting more electron density to the O_{15} atom. The nitrogen atoms of the urea moiety have negative charges due to the co-operative inductive effects of the hyperconjugative interactions such as $n(O_{15})\rightarrow \sigma^*(C_9-N_8/N_{10})$ and $n(N_8/N_{10})\rightarrow \sigma^*(C_9=O_{15})$, which increase the strong accumulation of electron density in the region of π-orbital lobes of N_{10}, N_8 and O_{15} atoms. They strongly decrease the accumulation of electron density on the opposite side of the π-orbital lobes which lies nearer to the C_9 atom and thereby creates the highest positive charge on the carbonyl carbon and large negative charges on the nitrogen atoms of the urea

12

moiety. The mesomeric effect in the urea moiety also develops positive charges on C_9 and the hyperconjugative effect due to the lone pairs of oxygen atoms gives positive character to C_6, C_7, C_{11} and C_{12} atoms. The H_{21}, H_{22} and H_{26} atoms have high positive natural atomic charges as compared to H_{23}, H_{24} and H_{27}, respectively, which indicates the proton donating abilities of H_{21}, H_{22} and H_{26} atoms and the H-bond formation gives more positive character to these atoms.

3.3 Vibrational analysis

FT-IR, FT-Raman and simulated vibrational spectra of UNMH are shown in Figs.3 and 4. The detailed vibrational assignment of the fundamental modes along with the predicted wavenumbers, IR and Raman intensities and mode descriptions with potential energy distribution (PED) in percentage for each mode are listed in Table 2.

- **Figure 3**

- **Figure 4**

- **Table 2**

The wavenumbers of the most of the fundamental modes observed in experimental spectra agree very well with the predicted wavenumbers. The Raman bands were experimentally observed with very low intensities. The significant decreases in Raman intensities are consistently attributable to the steric hindrance effect [49] of the molecular systems. The low values of PED for some prominent modes are due to the possible conformational difference and the different extents of H-bonding exist between the crystalline and gas phases of the sample.

3.3.1   C-H vibrations

The heteroaromatic system shows the CH stretching absorption bands in the region 3100-3000 cm^{-1} [50]. The CH stretching modes of UNMH were observed experimentally as a very strong intense but broad band at 3096 cm^{-1} in the IR spectrum and the Raman analogues appeared as very weak bands in the 3094-3070 cm^{-1} region. Normal coordinate analysis

13

predicted four bands for the υ(CH) mode with 99% PED contributions each at 3073 cm^{-1}, 3065 cm^{-1}, 3058 cm^{-1} and 3046 cm^{-1}. The fourth band corresponding to a scaled mode was absent in recorded spectra. The unassigned IR band which is observed as a highly intense and broad peak at 3175 cm^{-1} can be attributed to the CH stretching modes in the crystalline state. The up-shifting of this wavenumber and the shortening of the C-H bond as well as the presence of the sharp and high intense Raman peak observed around 1726 cm^{-1} clearly points to CH⋯O type interactions in the crystalline state. However, the phenyl CH bond has no contributions from the H-bonding in the isolated gas phase molecule. The substitution sensitive C-H in-plane and out-of-plane bending vibrations are expected in the range 1520-1000 cm^{-1} [50-53] and 1000-700 cm^{-1} [51], respectively. The C-H in-plane bending modes of UNMH are predicted to be in the spectral region 1626-1027 cm^{-1}. The weak bands observed in the IR spectrum at 964 cm^{-1} and 880 cm^{-1} as well as the strong bands at 810 cm^{-1} and 727 cm^{-1} are attributed to the out-of-plane CH wagging vibrations.

3.3.2 O-H vibrations

The absorption band corresponding to the non-hydrogen bonded OH stretching vibrations is expected in the region 3700-3584 cm^{-1} and the involvement of these bonds in H-bonding lowers the wavenumber to 3550-3200 cm^{-1} [53,54]. The medium strong broad IR band at 3571 cm^{-1} (Raman inactive) and the very strong peak observed in the IR at 3310 cm^{-1} and the corresponding very weak Raman band at 3308 cm^{-1} are attributed to the stretching vibrations of OH bonds attached to the ring. The wavenumbers corresponding to these modes were predicted with PED contributions of 100% at 3574 cm^{-1} and 97% at 3321 cm^{-1}, respectively. The lowering of stretching wavenumbers clearly indicate the involvement of the two bonds in O-H⋯O bonding interactions. The peaks corresponding to the in-plane OH bending vibrations are expected in the region 1440-1260 cm^{-1} [55, 56]. In UNMH, the COH in-plane bending modes are observed as medium strong to intense bands in the IR spectrum at 1469 cm^{-1} (1469 cm^{-1} in Raman), 1418 cm^{-1} (1415 cm^{-1} in Raman) and 1343 cm^{-1} (1334 cm^{-1} in Raman).

14

3.3.4 C=O vibrations

Carbonyl stretching modes are expected in the region 1750-1690 cm^{-1}. The bands observed both in the IR and Raman spectra at 1726 cm^{-1} and at 1683 cm^{-1} are attributed to the stretching modes of the free ($C_9=O_{15}$) and hydrogen bonded ($C_{12}=O_{13}$) carbonyl groups, respectively. The absence of H-bonding increases the *p* character to the carbonyl bond ($C_9=O_{15}$) of the urea ring and hence increases its double bond strength. As a result, the stretching absorption wavenumber of the $C_9=O_{15}$ bond increases slightly over the H-bonded carbonyl bond of the molecule. The involvement of the $C_{12}=O_{13}$ bond in O_{25}-H_{26}···O_{13} bonding interactions with the adjacent water molecule significantly lowers the stretching absorption wavenumber and such perturbative effect consequently gives more *s* character to the sigma bond of $C_{12}=O_{13}$, resulting in a slight increment in C=O double bond length hence the reduction in wavenumber as compared to the $C_9=O_{15}$ bond stretch. The calculated mode for the free carbonyl group of the molecule was up-shifted by 17 cm^{-1} over the corresponding fundamental mode. The lowering of the observed band position and the simultaneous appearance of the IR and Raman modes were obviously due to the intermolecular H-bonding at the carbonyl site of the urea ring in the crystalline system. The carbonyl wagging modes are identified in the IR spectrum at 810 cm^{-1} and 751 cm^{-1} and these modes of hydrogen bonded carbonyl group were found in the low wavenumber region also.

The strong band observed in the IR spectrum at 1113 cm^{-1} and a weak band at 1048 cm^{-1} are due to the C-O stretching modes. The peaks corresponding to the OCC/N in-plane bending modes are observed in the Raman spectral region 1165-656 cm^{-1} and that of out-of-plane bending modes are in the region 534-183 cm^{-1}. The twisting and torsional vibrations about the C-O bonds were identified using the DFT calculations.

3.3.5 N-H vibrations

The N-H stretching modes of urea are expected in the region 3500-3000 cm^{-1} [18, 21]. The calculated structure for the molecule was free from N-H···O bonding. This was revealed from the NH stretching modes of the molecule which were scaled to be at 3521 cm^{-1} and

15

3483 cm^{-1}. But in the crystalline state, the intervention of NH bonds in hydrogen bonding can be easily identified by the presence of red-shifted stretching absorption peaks in the IR spectrum at 3502 cm^{-1} and 3467 cm^{-1}. The observed band positions and intensities of these modes point to the presence of intramolecular N-H···O type interactions in the crystalline state. The H-bonding at the NH sites also affected the vibrations of the CNH bending modes in the crystalline phase. The strong band observed in the IR spectrum at 1395 cm^{-1} is attributed to the in-plane CNH bending mode and the corresponding calculated mode is found to be at 1353 cm^{-1}. The medium strong IR peak at 419 cm^{-1}, very weak Raman peaks at 410 cm^{-1} and calculated modes below 475 cm^{-1} show contributions from the NH wagging modes.

3.3.6   Ring system vibrations

The butterfly mode due to the combined vibrations of the benzene and the fused cyclopentanone ring of UNMH was calculated to be at 145 cm^{-1}.

3.3.6.1 *Benzene ring:*

The CC stretching vibrations of benzene derivatives are generally observed in the IR region 1625-1430 cm^{-1} [57] and the C=C stretching absorptions appeared as doublets in the region 1625-1575 cm^{-1} [53]. The two well resolved weak sharp bands observed in the Raman spectrum at 1605 cm^{-1} and 1590 cm^{-1}, corresponding to the strong IR bands at 1619 cm^{-1} and 1603 cm^{-1} are assigned to the coupled modes of CC ring stretching and bending vibrations. The occurrence of these bands in recorded spectra obviously indicates the strong π-conjugation in the benzene ring. The very weak band observed at 1523 cm^{-1} in the IR spectrum is assigned to the CC semi-circle stretching of the benzene ring. The CCC trigonal bending and the ring breathing modes of substituted benzene are generally observed around 1000 cm^{-1} and 800 cm^{-1}, respectively. The peaks observed in the IR spectrum at 1084 cm^{-1} and 964 cm^{-1} are assigned to the CCC trigonal and the CCC ring breathing modes, respectively. The weak IR band observed at 880 cm^{-1} can be assigned as the ring puckering mode which is calculated to be coupled with the out-of-plane CH wagging mode. The DFT calculations predicted the CCC out-of-plane bending modes of the benzene ring at 543 cm^{-1}

and at 244 cm^{-1}. The peak corresponding to the twisting mode of the benzene ring of UNMH is observed in the IR spectra at 454 cm^{-1} and this mode was calculated to be with the PED of 64% at 453 cm^{-1}. The Raman band at 336 cm^{-1} can be assigned to the torsional mode of the benzene ring.

3.3.6.2 *Fused cyclopentanone ring:*

The CC ring stretching mode is identified experimentally in the IR region 1418-546 cm^{-1}. The DFT calculation showed the prominent contributions of υ(CC) modes at 1246 cm^{-1}, 1194 cm^{-1} and 1027 cm^{-1}. The strong peak observed at 546 cm^{-1} in the IR spectrum is assigned to the skeletal bending modes of the central ring. It is found from DFT calculations that the CCC bending mode was weakly coupled with the prominent stretching vibrations originated from the CC and the C=O bonds attached to the fused cyclopentanone ring. The wavenumbers predicted at 543 cm^{-1} and 244 cm^{-1} are assigned to the inter-ring bond bending modes of CCC linkages of the benzene and the fused central five-membered ring. The ring twisting and the torsional modes were assigned using the result of force-field calculations.

3.3.6.3 *Substituted urea moiety ring:*

Stewart [21] assigned the asymmetric and symmetric CN bond stretching vibrations of urea around 1468 cm^{-1} and 1005 cm^{-1}, respectively. The bands observed in FT-IR spectrum at 1294 cm^{-1}, 1084 cm^{-1} and 1010 cm^{-1} as well as the Raman bands at 1295 cm^{-1}, 1084 cm^{-1}, 1013 cm^{-1} and 974 cm^{-1} are assigned to the CN stretching modes of UNMH as the PED showed prominent contributions at these wavenumbers. These modes are also coupled to the NH bending coordinate in the ring. The CNC twisting modes of the ring are observed as the very strong IR band at 751 cm^{-1} and the very weak Raman peak at 750 cm^{-1} and the theoretically scaled modes were predicted to be at 750 cm^{-1} with PED contributions of 15%. The torsional modes of the ring were calculated to be in the theoretical spectral region of 199-25 cm^{-1}.

3.3.7 Vibrations of the water molecule

The OH stretching vibrations of the water molecule appeared in the region 3700-3584 cm^{-1} [58]. The asymmetric and the symmetric O-H stretching absorptions are observed as a very weak band at 3656 cm^{-1} and a weak band at 3431 cm^{-1} in the IR spectrum, respectively, and the Raman counterparts were absent. These band positions were predicted in the calculated spectra with very low Raman intensities at 3720 cm^{-1} with PED of 100% and at 3410 cm^{-1} with PED of 97%. The red shifting in wavenumbers are clearly due to the involvement of the water molecule in the hydrogen bonding interactions with the adjacent ring system. The bending mode of the water molecule is expected around 1595 cm^{-1} [58]. In UNMH, the bending vibration of the water molecule interfered strongly with its hydrogen bonding interactions with the carbonyl group. The very strong IR peak observed at 1683 cm^{-1} is assigned to the coupled vibrations of the carbonyl and hydrate groups through the H-bonding. The medium strong peak at 1647 cm^{-1} and a strong peak at 1619 cm^{-1} are assigned as HOH scissoring modes.

3.3.8 Hydrogen bonding vibrations

The H-bonding interactions in UNMH produce drastic effects in the vibrational modes of the molecular system as they are strongly coupled with other vibrational modes of the system. The wavenumbers of the substituted urea ring vibrations are sensitive to the strength of H-bonding at the NH and the C=O sites in the crystalline state. These H-bonding interactions enhance the intramolecular charge transfer by the simultaneous introduction of more electrons to the electron negative groups and enhance the weakening of the bond which resulted in the red shifting of absorption wavenumbers. The enhancement in the IR stretching intensities of the C=O bond and the OH bonds of the water molecule signifies the extent of intramolecular polarization between the ring system and the water moiety. From the theoretical PED contributions at 257 cm^{-1} the very weak peak observed in the Raman spectrum at 256 cm^{-1} can be assigned to the H-bonded torsional oscillations of $H_{27}\cdots O_{25}$-$H_{26}\cdots O_{13}$ bond formed between the water molecule and the ring system. The strength of these interactions can be estimated from the calculated PED contributions of 32% for the stretching

vibrations due to the pseudo bond $O_{13}\cdots H_{21}$ at 321 cm^{-1}. The O$\cdots$H hydrogen bond stretching modes were particularly active in the low wavenumber region below 375 cm^{-1} as revealed by their prominent PED contributions.

3.4 Frontier orbitals and MEP surface studies

The frontier molecular orbitals give salient information for the electronic structure study. Fig.5(a) depicts the molecular orbitals of the highest occupied molecular orbital (HOMO) and the lowest unoccupied molecular orbital (LUMO) of UNMH molecule. The HOMO spans entirely over the molecule except the C_1-C_2, C_2-C_3, C_6-C_7 and C-H bonds as well as the O_{25}-H_{27}, bonds of hydrate group. The LUMO is distributed over the urea-ninhydrin ring excluding the C_3-H_{19}, C_7-C_{11}, C_7-O_{16}-H_{22}, N_8-H_{24}, N_{10}-H_{23}, C_7-N_8, N_8-C_9, O_{14}-H_{21} and the C_9=O_{15} bonds of the ring as well as the water molecule. The charge transfer transition from HOMO to LUMO clearly specifies the strengthening of urea-ninhydrin ring system. The HOMO and LUMO energies as well as the HOMO-LUMO energy gap for UNMH are estimated to be -7.1024 eV, -2.4259 eV and 4.6765 eV, respectively. Since the HOMO and the LUMO are entirely overlapped in the urea-ninhydrin ring, it results in consistent weakening of both the bonds in the ring system. The charge transfer interactions are then facilitated because of the weakening of bonds which causes the lowering of LUMO and enhancement of the HOMO energy levels.

- **Figure 5**

The global reactivity descriptors can be used to describe the molecular properties. The descriptors such as the ionization potential (IP) and the electron affinity (EA) were approximated by the energies of the HOMO and the LUMO, respectively, using Koopman's theorem [59], as $-E_{HOMO} \approx IP$ and $-E_{LUMO} \approx EA$. The stability of the molecule can be interpreted from the value of chemical hardness (η) by the relation [60], $\eta = (IP - EA)/2$. The electronegativity, χ is calculated from the relation, $\chi = (IP + EA)/2$ and the negative value of χ gives the chemical potential of the molecular system. The electrophilicity index

19

[61], $\omega = \mu^2/2\eta$ measures the energy lowering due to the maximum electron flow between donor and acceptor orbitals. The total energy change [62] is calculated from the relation, $\Delta E_T = -\eta/4$. The global softness [63] value expresses the degree of chemical reactivity of the molecule and is calculated using the relation, $S = 1/2\eta$. The energy gain or loss in a donor-acceptor charge transfer is determined from the overall energy balance, $\Delta E = EA - IP$. The calculated global reactivity descriptors for the molecule of UNMH are listed in Table 3.

- **Table 3**

Fig.5(b) shows the molecular electrostatic potential (MEP) surface plot of UNMH. The MEP surface of UNMH was generated by mapping the electrostatic potential onto the isosurface (±0.0100 au) of molecular electron density. The red coloured region signifies the most negative electrostatic potential while the blue region indicates the maximum positive electrostatic potential. The positive potential region is spread around all hydrogen atoms. Stronger negative potential is found in the region of the oxygen and nitrogen atoms due to their lone pair electrons and this region will be more susceptible to the strong electrophilic attack. An electron rich bridge with negative electrostatic potential is seen over these atoms in the molecule. The steric hindrance effect may also make the space between the urea moiety and the hydroxyl groups to an electron denser region. The MEP plot confirms the existence of intramolecular H-bond sites in UNMH.

3.5 UV-Vis-NIR studies

Recorded spectra of the sample in solid phase and theoretical spectra in gas and water phases are shown in Fig.6.

- **Figure 6**

The experimental spectrum has a strong intense absorption peak at 335 nm, less intense but sharp peaks appeared in the region 199-383 nm and beyond which a broad band at 408 nm. The absorption cut-off wavelength of the crystalline phase is observed around 460 nm. The

20

absorption edge of the optical spectrum of UNMH crystal is being red-shifted as compared to that of urea [26] and ninhydrin [32]. Hence the inherited molecular symmetry can be used to explain the observed optical absorption differences. The strong $\pi \rightarrow \pi^*$ charge transfer transitions are responsible for the red-shifting of the wavelength in the crystalline UNMH. The red shifted π-electron transitions by π-conjugations point out the extent of H-bonding interactions in the crystalline phase and thus the third-order nonlinearity of UNMH.

The TD-DFT results of the gas and the water phase electronic absorptions of UNMH were summarized in Table 4.

- **Table 4**

The absorption maxima calculated for the gas phase and water phase of UNMH were 300.94 nm and 292.10 nm, respectively. The electronic excitations from HOMO-1 to LUMO orbitals with the contributions of 89.4% for the gas phase and 90.9% for the water phase were responsible for the absorption maxima at these wavelengths. The absorption at 286.56 nm for the gas phase was due to the charge transitions from HOMO-2 to LUMO and in the case of the water phase, the HOMO-3$\rightarrow$LUMO transition was responsible for the absorption around 268.04 nm. The HOMO$\rightarrow$LUMO transition gives absorption at 346.57 nm for the gas and 335.73 nm for the water phases, which are found to be contributed with low oscillator strengths because of the hyperconjugative interactions in the ring system. The absorption behaviour of the isolated gas and water phases of the molecule can be attributed to the n$\rightarrow \pi^*$ type-transitions due to the carbonyl bond, which is also revealed by the NBO analysis. The calculated absorption maximum wavelength for the gas phase is larger than that of the solution phase indicating the existence of intensive n$\rightarrow \pi^*$ hyperconjugation due to the lone pair electrons of the oxygen and the nitrogen atoms of the molecule in the solution phase of UNMH.

3.6 Second-order NLO study

The polarization changes associated with a molecule when it is subjected to an intense electric field leads to produce its nonlinear effect. The polarizability changes can be expressed as

$$P(E) = \alpha_{ij}E_j + \beta_{ijk}E_jE_k + \gamma_{ijkl}E_jE_kE_l + \cdots \tag{11}$$

where $P(E)$ is the induced electrical polarization, α_{ij} is the ij component of the isotropic polarizability tensor, β_{ijk} is the ijk component of molecular first-hyperpolarizability and γ_{ijkl} is the $ijkl$ component of the molecular second-hyperpolarizability. The optimization and the perceptive understanding of the NLO properties of organic materials are easily interpreted from their molecular hyperpolarizabilities.

The static as well as the dynamic first-order hyperpolarizabilities (β_{total}) and static second- hyperpolarizabilty ($\langle\gamma\rangle$) of title molecule and the corresponding values of the most widely used standard organic molecule, urea were calculated using DFT/B3LYP method. The results of all the calculations were listed in Table ST3 (*Supporting Information*). The calculated static first-hyperpolarizability of UNMH in gas phase with cc-pVTZ basis set was 3.6837×10^{-30}esu, which is 5.57 times that of urea (0.66085×10^{-30}esu) and 1.21 times greater than that of anhydrous urea ninhydrin (AUN). Hence, the presence of the water molecule increases the nonlinear responses of the urea-ninhydrin ring system by the possibilities of various H-bonding interactions other than by the anhydrous one. The static first-hyperpolarizability of UNMH was also computed with the 6-311++G(d,p) basis set and compared with the reported static β value of ninhydrin [33] which was calculated using the same level of theory. At this level the static β_{total} value estimated for UNMH was 2.8813×10^{-30} esu, which is 1.18 times greater than that of the reported value for ninhydrin molecule. The intramolecular interactions especially the strong hyperconjugations due to H-bonding which cause an acentricity in the electron charge density distribution of the isolated gas-phase UNMH molecule are responsible for its non-zero value of the hyperpolarizability components. The predicted dynamic first-hyperpolarizability with the B3LYP/cc-pVTZ level

22

for UNMH at the Nd:YAG laser frequency (λ=1064 nm) for electro-optical Pockels effect, $\beta(-\omega;\omega,0)$ was 4.1308$\times10^{-30}$ esu, and for the second harmonic generation, $\beta(-2\omega;\omega,\omega)$ was 5.2751$\times10^{-30}$ esu which were 5.91 and 7.33 times, respectively, as that of the isolated gas phase urea molecule at the same level of theory. The estimated dynamic β values for UNMH are larger than those of the anhydrous urea-ninhydrin molecule also. The predicted values of the mean static and dynamic polarizabilities for UNMH were found to be 21.2263$\times10^{-24}$ esu and 21.4938$\times10^{-24}$ esu, respectively. The total dipole moment of the molecule (4.0484 Debye) is 1.08 times greater than that of urea (3.7321 Debye) which indicates the superior polar nature of UNMH molecule.

The predicted hyperpolarizability values are computed for the isolated gas phase global minimum configuration of the monomeric structure and the values depend on its conformation. This can be interpreted from the calculated hyperpolarizability values (Table ST3, *Supporting Information*) of the other structural configuration of urea ninhydrin monohydrate (UNMHC) which has an additional NH$\cdots$O bonding different from UNMH. Also, the UNMHC was energetically less stable and whose NLO responses were smaller than UNMH. The hyperpolarizability values can change in accordance with the structural diversity and the conformational flexibility of molecules in a crystal. The centrosymmetric crystalline pattern of UNMH can also be related to the conformational preferences of each molecule that can bring substantial changes in bulk susceptibility.

SHG is forbidden within the electric dipole approximation in centrosymmetrical molecule or materials. The overall second-order NLO response vanishes in the electric dipole approximation owing to the presence of inversion symmetry. The response of centrosymmetric molecules to an external field is given by $P(-E) = -P(E)$. This relation expresses the requirement that the induced polarization of centrosymmetric molecules is opposite and of equal of magnitude when the field is reversed. In order for equation (11) to satisfy this condition, all coefficients of even powers of E have to be equal to zero. Hence,

23

only noncentrosymmetric molecules have a nonzero β value, since then $P(-E) \neq -P(E)$. The relationship between the polarizabilities of different order and the corresponding susceptibilities involve accounting for molecular orientations in the material and for local field factors [64]. The nature of nonlinear optical interactions is depends on the magnitude and form of the nonlinear susceptibility tensor. Generally, the nth order susceptibility $\chi^{(n)}$ is a tensor of $(n+1)^{th}$ rank. At the microscopic level the hyperpolarizabilities β (3rd rank tensor) and γ (4th rank tensor) behave similarly to the macroscopic susceptibilities, $\chi^{(2}$ and $\chi^{(3)}$, respectively. According to the dipolar approximation and symmetry consideration the nonlinear susceptibilities $\chi^{(n)}$ with even n are zero for a centrosymmetric material. So, even order nonlinear optical effects can be observed only in noncentrosymmetric material, or in cases where centrosymmetry is broken. In the case of materials lacking a centre of symmetry, the nonlinearity arises due to the combinations of $\chi^{(2)}$ and $\chi^{(3)}$. The dominating effect of $\chi^{(2)}$ in certain cases leads to their second-order NLO property. For a material with a centre of symmetry all the components of second-order susceptibility tensor ($\chi^{(2)}$) vanish and the nonlinearity is generally dominated by the third-order susceptibility ($\chi^{(3)}$). The requirement of noncentrosymmetry is not restricted to the molecular level but also applies to the macroscopic nonlinear susceptibility, $\chi(2)$, which means that the second-order NLO molecules have to be organized in a noncentrosymmetric alignment. This is not the case of UNMH crystal which possesses an inversion centre and so, it cannot produce the second harmonic of the fundamental, and so the SHG efficiency must be about zero.

Kurtz and Perry powder SHG measurement was employed to determine the second-order NLO property of the sample. In this method, the finely powdered crystalline samples were packed in a microcapillary glass-tube of uniform bore. The laser pulses having a pulse width of 10 ns at a repetition rate of 10 Hz from a Q-switched Nd-YAG laser source of fundamental wavelength of 1064 nm were used for the SHG measurement. The input beam energy of the laser was 1.2 mJ/pulse. The laser beam was focused by a plano-convex lens of focal length 20 cm and the beam was then converged into the sample taken in the micro-

capillary. The output from the sample was collected in the transverse direction using a 532 nm monochromator and was then detected by a photomultiplier tube which converts the intensities of the generated signal into the voltage at the digital storage oscilloscope. The sample has showed a near-zero signal voltage at the oscilloscope. So the SHG efficiency of the crystal was found to be near-zero. This can be attributed to the presence of a symmetry centre in the crystal which eliminates the possibility of generation of the second harmonic of light from it due to the cancellation of non-linear polarization components.

3.7   Third-order NLO study

Third-order nonlinearity is a universal property found in any material regardless of its spatial symmetry. This non-linearity is the lowest-order non-vanishing for a broad class of centrosymmetric materials, where all the even-order nonlinear susceptibilities are identically equal to zero for symmetry reasons. The macroscopic third-order susceptibility or the microscopic second- hyperpolarizability term is used to describe the third-order NLO response of a material. In the case of centrosymmetric UNMH, the static value of the second-hyperpolarizability (γ) calculated at DFT/B3LYP/cc-pVTZ method was 7.8308×10^{-36} esu which is 11.56 times that of gas phase urea (0.67765×10^{-36} esu) molecule. The predicted γ value of urea can also be compared with its experimentally determined value obtained from electric-field-induced second harmonic generation measurement in water solution which was 7.1×10^{-36}- 12.7×10^{-36} esu [28].

The non-linear absorption is an important class of third-order NLO process. The open-aperture Z-scan study was employed for measuring the non-linear absorption property of UNMH. Z-scan is based on the nonlinear transverse modification of the focused Gaussian laser beam by a sample through a region of modulated intensity created by a convex lens throughout its focal length. The resulting intensity variation is experienced by the sample which is translated through the laser beam direction around the focal point of the lens. As the sample passes through the focus of the laser beam, changes in its transmittance due to nonlinear absorption is measured by an open aperture method. Here the transmitted beam

25

from the sample is completely focused directly into the detector, ie., no aperture to curtail the beam profile and hence the name open-aperture. Depending on the nonlinearity of the sample, the transmittance either increases or decreases about the focus of the incident beam and the detector receives more or less than the linear transmittance, yielding a hump or dip in the curve of transmittance as a function of the sample position.

The nonlinear absorption of the water solution of UNMH is measured with the open-aperture Z-scan technique using 532 nm excitation wavelength with laser pulses of 5 ns pulse duration obtained from a Q-switched Nd:YAG laser source. The laser output from the source was spatially filtered to obtain a perfect Gaussian beam profile which is used as incident laser beam for the measurement. The beam is then focused using a plano-convex lens to determine its focal point. The direction of beam propagation is taken as the z-axis, and the focal point is taken as z=0. The sample taken in a 1 mm path length glass cuvette was then mounted on a programmable linear translation stage, and was able to move along the z-axis with respect to the focus of the lens. The sample is thus exposed to the beam at a position z between the lens and the focal point. The input energy reaching the sample and the transmitted energy from the sample are measured using two pyroelectric energy probes. The input energy used for the laser irradiation was 35 μJ. The sample is then moved in small steps from -z to +z, towards the focus and beyond the focus, and the transmission is measured in each step. At each of these positions, the sample has experienced different laser intensities, and the highest intensity is measured when the sample was at the focal point. The interval between successive laser pulses was kept sufficiently large to allow for complete thermal relaxation of the sample between adjacent laser pulses. The whole experiment was automated using a PC. If a spatially resolved Gaussian laser beam is used, then each z-position will correspond to input laser fluence. Thus from the open-aperture Z-scan data, it is possible to draw a graph connecting the input laser fluence and the sample transmission. The nature of the graph will reveal the absorptive non-linearity of the system.

26

Fig.7(a) shows the open aperture Z- scan experimental data (circles) and the fitted Z-scan curve (solid curve) obtained for the sample in water solution under an excitation wavelength of 532 nm using laser pulses of 5 ns pulse duration.

- **Figure 7**

Normalized transmittance result of the open aperture Z-scan indicates that the sample has non-linearity due to reverse saturable absorption, RSA (also known as excited state absorption). Linear transmission of the sample was 60% at the excitation wavelength. The RSA coefficient for the sample was calculated from the best numerical fit to the Z-scan experimental data which is obtained using the equation for open aperture normalized transmittance given by

$$T = \left(\frac{(1-R)^2 e^{-\alpha L}}{\sqrt{\pi}\, q_0}\right) \int_{-\infty}^{+\infty} ln\left[1 + q_0 e^{-t^2}\right] dt \tag{1}$$

where T is the net transmission of the sample, L and R are the length and surface reflectivity of the sample, respectively and α is the linear absorption coefficient. The parameter q_0 in equation (1) is given by $\beta(1-R)\, I_0 L_{eff}$, where β is the RSA coefficient, I_0 is the on-axis peak laser intensity and L_{eff} is given by $(1 - e^{-\alpha L})/\alpha$.

The RSA coefficient obtained for urea ninhydrin monohydrate is 19×10^{-11} m/W. For ninhydrin itself a value of 2.5×10^{-11} m/W [31] was found under similar experimental conditions as that of the sample under study. The addition of urea and water moieties to the ninhydrin enhances its non-linear absorption mechanism. The peculiarities of the molecular structure such as the presence of weak H-bond in the tricyclic ring system as well as the moderate H-bonds between the ring system and the water moiety, the efficient intra molecular charge transfer interactions with low delocalization energies and the intensive π-conjugation, can make the molecule highly polarized that may increase the third-order non-linearity of the crystal. UNMH exhibits a strong reverse saturable absorption and the calculated RSA efficiency is comparable to other nonlinearly absorbing NLO materials [65-67] having optical limiting property. The optical limiting behaviour (i.e., the decrement in the

27

sample's transmission with the increment in the input laser fluence) of the sample is depicted in Fig.7(b). The nonlinear optical absorption effect in the sample results in its strong optical limiting property. The optical limiting performance of UNMH can be utilized to fabricate devices for protecting eyes and sensors from high-intensity laser beams.

Conclusion

The structural, vibrational and nonlinear properties of UNMH have been investigated using computational simulations and by experimental techniques. Quantum chemical DFT calculations have been used to assign the normal modes in the vibrational spectra associated with the observed spectroscopic bands. The energetic importance of the intramolecular H-bond interactions were estimated using the NBO analysis method. The monomer structure is stabilized by the formation of weak O-H⋯O and moderate O-H⋯O intramolecular non-planar hydrogen bonds. The Kurtz and Perry powder measurement study confirmed the near-zero SHG efficiency of the crystal. The presence of a symmetry centre in the crystal eliminates the possibility of generation of the second harmonic of light from it. The DFT calculation predicted the cubic nonlinearity with non-zero hyperpolarizability components for the isolated gas phase molecule. UNMH exhibited third order nonlinearity due to RSA and the RSA coefficient was 19×10^{-11} m/W for nano second laser pulse irradiation. The crystal has excellent absorption in the ultraviolet region and its absorption edge is shifted to the visible region. The red shifting in the wavenumber of the OH stretching mode and bathochromic shift in electronic absorption maxima are caused by the through-space hyperconjugative interactions due to the carbonyl bonds of UNMH. The measured third-order nonlinear properties and UV-Vis-NIR absorption studies confirm its suitability for optical limiting applications in the visible and near infrared region. The intermolecular NH⋯O and CH⋯O type bond formation along with the intramolecular OH⋯O bonding together resulted in the significant enhancement of the π-conjugation length within the molecular system, and consequently the third-order NLO property of the centrosymmetric crystal system. The experimental and theoretical data of the studied crystal can be used to modify its structural,

28

electronic, optical and physiochemical properties with the possibilities of molecular engineering in designing novel molecular architectures with enhanced NLO responses according to the requirements of technological applications.

Acknowledgement

References

[1] J. Zyss, J. L. Oudar, Relations between microscopic and macroscopic lowest-order optical nonlinearities of molecular crystals with one- or two- dimensional units, Phys. Rev. A 26 (1982) 2028-2048.

[2] R. D. Wampler, N. J. Begue, G. J. Simpson, Molecular design strategies for optimizing the nonlinear optical properties of chiral crystals, Cryst. Growth Des 8(8) (2008)2589-2594.

[3] J. L. Oudar, J. Zyss, Structural dependence of nonlinear-optical properties of methyl-(2,4-dinitrophenyl)-aminopropanoate crystals, Phys. Rev. A 26 (1982) 2016-2027.

[4] M. C. Etter, Aggregate structures of carboxylic acids and amides, Isr. J. Chem. 25 (1985) 312-319.

[5] M. C. Etter, A new role for hydrogen-bond acceptors in influencing packing patterns of carboxylic acids and amides, J. Am. Chem. Soc. 104 (1982) 1095-1096.

[6] B. F. Levine, C. G. Bethea, Effects on hyperpolarizabilities of molecular interactions in associating liquid mixtures, J. Chem. Phys. 65 (1976) 2429-2438.

[7]   GUO Wensheng, GUO Fang, WEI Chunsheng, LIU Qitao, ZHOU Guangyong, WANG Dong, SHAO Zhongshu, SHG from centrosymmetric supermolecular crystal, SCIENCE IN CHINA (Series B) 45(3) (2002) 267-274.

[8]   G. J. Ashwell, G. Jefferies, D. G. Hamilton, D. E. Lynch, M. P. S. Roberts, G. S. Bahra, C. R. Brown, Strong second-harmonic generation from centrosymmetric dyes, Nature 375 (1995) 385-388

[9]   T. U. Devi, N. Lawrence, R. R. Babu, S. Selvanayagam, H. S. Evans, K. Ramamurthi, Characterization of a newly synthesized organic nonlinear optical crystal: urea ninhydrin monohydrate, J. Cryst. Growth 311 (2009) 3485-3490.

[10]   J. E. Worsham Jr., H. A. Levy, S. W. Peterson, The positions of hydrogen atoms in urea by neutron diffraction, Acta Cryst. 10 (1957) 319-323.

[11]   S. Swaminathan, B. M. Craven, R. K. McMullan, The crystal structure and molecular thermal motion of urea at 12, 60 and 123 k from neutron diffraction, Acta Cryst. B 40 (1984) 300-306.

[12]   R. C. Medrud, The Crystal Structure of Ninhydrin, Acta Cryst. B 25 (1969) 213-220.

[13]   A. Masunov and J. J. Dannenberg, Theoretical study of urea. I. Monomers and dimmers, J. Phys. Chem. A 103(1) (1999) 178-184.

[14]   T. U. Devi, N. Lawrence, R. R. Babu, K. Ramamurthi, G.Bhagavannarayana, Growth of ninhydrin single crystal and its characterization, Spectrochimica Acta Part A 71 (2009) 1667-1672.

[15]   R. Ananthakrishnan, The Raman spectra of crystal powders. IV Some organic and inorganic compounds, Proc. Indian Acad. Sci. (A) 5 (1937) 200-221.

[16]   D. D. V. Slyke, P. B. Hamilton, The synthesis and properties of ninhydrin ureide, J. Biol. Chem. 150 (1943) 471-476.

[17]   T. Prasanyaa, V. Jayaramakrishnan, M. Haris, Antimicrobial activity and second harmonic studies on organic non-centrosymmetric pure and doped ninhydrin single crystals, Spectrochimica Acta Part A 104 (2013) 110-113.

[18] R. Keuleers, H. O. Desseyn, B. Rousseau, C. V. Alsenoy, Vibrational analysis of urea, J. Phys. Chem. A 103 (1999) 4621-4630.

[19] D. A. Dixon, N. Matsuzawa, Density functional study of the structures and nonlinear optical properties of urea, J. Phys. Chem. 98 (1994) 3967-3977.

[20] R. Li, H. Sui, P. Liu, L. Chen, J. Cheng, B. Zhao, Vibrational spectroscopy and density functional theory study of ninhydrin, Spectrochimica Acta Part A 136 (2015) 1642-1648.

[21] J. E. Stewart, Infrared absorption spectra of urea, thiourea, and some thiourea-alkali halide complexes, J. Chem. Phys. 26 (1957) 248-254.

[22] S. K. Kurtz, T. T. Perry, A powder technique for the evaluation of nonlinear optical materials, J. Appl. Phys. 39 (1968) 3798-3813.

[23] D. Bäuerle, K. Betzler, H. Hesse, S. Kapphan, P. Loose, Phase-matched second harmonic generationin urea, Phys. Stat. Sol. (a) 42 (1977) K119-K121.

[24] K. Betzler, H. Hesse, P. Loose, Optical second harmonic generation in organic crystals: urea and ammonium-malate, J. Mol. Struct. 47 (1978) 393-396.

[25] J. M. Halbout, S. Blit, W. Donaldson, C. L. Tang, Efficient phase-matched second-harmonic generation and sum-frequency mixing in urea, IEEE J. Quantum Electronics 15 (1979) 1176-1180.

[26] C. Cassidy, J. M. Halbout, W. Donaldson, C. L. Tang, Nonlinear optical properties of urea, Opt. Commun. 1979 (29) 243-246.

[27] K. Kato, High-efficiency high-power UV generation at 2128 Å in urea, IEEE J. Quantum Electronics 16 (1980) 810-811.

[28] I. Ledoux, J. Zyss, Influence of the molecular environment in solution measurements of the second-order optical susceptibility for urea and derivatives, J. Chem. Phys. 73 (1982) 203-213.

[29] H. Reis, M. G. Papadopoulos, R. W. Munn, Calculation of macroscopic first-, second-, and third-order optical susceptibilities for the urea crystal, J. Chem. Phys. 109 (1998) 6828-6838.

[30] T. Pluta, A. J. Sadlej, Electric properties of urea and thiourea, J. Chem. Phys. 114 (2001) 136-146.

[31] N. Vijayan, J. Philip, D. Haranath, B. Rathi, G. Bhagavannarayana, S. K. Halder, N. Roy, M. S. Jayalakshmy, S. Verma, Bulk growth of ninhydrin single crystals by solvent evaporation method and its characterization for SHG and THG applications, Spectrochimica Acta Part A 122 (2014) 309-314.

[32] D. Sajan, T. U. Devi, K. Safakath, R. Philip, I. Němec, M. Karabacak, Ultrafast optical nonlinearity, electronic absorption, vibrational spectra and solvent effect studies of ninhydrin, Spectrochimica Acta Part A (2013) 109 331-343.

[33] M. Arivazhagan, D. A. Rexalin, Molecular structure, vibrational spectral analysis, NBO, HOMO-LUMO and conformational studies of ninhydrin, Spectrochimica Acta Part A 104 (2013) 451-460.

[34] J. C. Dobrowolski, R. Kołos, J. Sadlej, A. P. Mazurek, Theoretical and IR-matrix isolation studies on the urea and urea-D_4, -^{13}C, and -$1,3$-$^{15}N_2$ substituted molecules, Vib. Spectrosc. 29 (2002) 261-282.

[35] M. Spoliti, G. Perrone, L. Bencivenni, A. Pieretti, A. Grandi, F. Ramondo, Computational and vibrational spectroscopy study of the microclusters of C_2 symmetry urea molecule in the ^1A electronic ground state, J. Mol. Struct. (THEOCHEM) 756 (2005) 113-126.

[36] M. S. Miao, V. E. V. Doren, R. Keuleers, H. O. Desseyn, C. V. Alsenoy, J. L. Martins, Density functional calculations of the structure of crystalline urea under high pressure, Chem. Phys. Lett. 316 (2000) 297-302.

[37] M. S. Bahae, A. A. Said, T. H. Wei, D. J. Hagan, E. W. V. Stryland, Sensitive measurement of optical nonlinearities using a single beam, IEEE J. Quantum Electronics 26 (1990) 760-769.

[38] A. D. Becke, Density- functional thermochemistry. III. The role of exact exchange, J. Chem. Phys. 98(7) (1993) 5648-5652.

[39] C. Lee, W. Yang, R. G. Parr, Development of the Colle-Salvetti correlation-energy formula into a functional of the electron density. Phys. Rev. B 37 (1988) 785-789.

[40] J. B. Foresman, A. Frisch, Exploring Chemistry with Electronic Structure Methods; second ed., Gaussian Inc., Pittsburgh, USA, 1996.

[41] T. H. Dunning Jr., Gaussian basis sets for use in correlated molecular calculations. I. The atoms boron through neon and hydrogen, J. Chem. Phys. 90 (1989) 1007-1023.

[42] M. J. Frisch, G. W. Trucks, H. B. Schlegel, G. E. Scuseria, M. A. Robb, J. R. Cheeseman, G. Scalmani, V. Barone, B. Mennucci, G. A. Petersson, et al. Gaussian 09, Revision A.02, Gaussian, Inc.: Wallingford, CT, 2009.

[43] R. Dennington, T. Keith, J. Millam, Gaussview, Version 5, Semichem, Inc.: Shawnee Mission, KS, 2009.

[44] E. D. Glendening, A. E. Reed, J. E. Carpenter, F. Weinhold, et al. NBO Version3.1. TCI, University of Wisconsin, Madison, 1998.

[45] T. Sundius, Scaling of ab initio force fields by MOLVIB, Vib. Spectrosc. 29 (2002) 89-95.

[46] M. J. Frisch, G. W. Trucks, H. B. Schlegel, G. E. Scuseria, M. A. Robb, J. R. Cheeseman, G. Scalmani, V. Barone, B. Mennucci, G. A. Petersson, et al. Gaussian 09, Revision C.01, Gaussian, Inc.: Wallingford, CT, 2010.

[47] R. Krishnan, J. S. Binkley, R. Seeger, J. A. Pople, Self-consistent molecular orbital methods. XX. A basis set for correlated wave functions, J. Chem. Phys. 72(1) (1980) 650-654.

[48] R. M. Stevens, E. Switkes, E. A. Laws and W. N. Lipscomb, Self-consistent-field studies of the electronic structures of cyclopropane and benzene, J. Am. Chem. Soc. 93 (1971) 2603-2609.

[49] K. M. Gough, C. Lupinetti, R. Dawes, Computation and interpretation of Raman scattering intensities, J. Comput. Meth. in Science and Engineering 4 (2004) 597-609.

[50] G. Varsányi, Assignment for Vibrational Spectra of Seven Hundred Benzene Derivatives, vol. 1-2, Akadémiai Kiadó, Budapest, 1973.

[51] N. P. G. Roeges, A Guide to Complete Interpretation of Infrared Spectra of Organic Structures, Wiley, New York, 1994.

[52] L. J. Bellamy, The Infrared Spectra of Complex Molecules; Chapman and Hall Ltd., London, 1975.

[53] G. Socrates, Infrared Characteristic Group Frequencies, Wiley-Inter Science Publication, New York, 1990.

[54] G. Dhanaraj, M. R. Srinivasan, H. L. Bhat, J. Raman Spectrosc. 22 (1991) 177-181.

[55] R. M. Silverstein, F. X. Webster, Spectrometric Identification of Organic Compounds, John Wiley and Sons, Inc., New York, 2003.

[56] N. B. Colthup, L. H. Daly, S. E. Wiberley, Introduction to infrared and Raman spectroscopy; Academic Press, New York, 1990.

[57] D. N. Sathyanarayana, Vibrational Spectroscopy: Theory and Applications, New Age International Publishers, New Delhi, 2004.

[58] B. Smith, Infrared Spectral Interpretation, a Systematic Approach, CRC, Washington, DC, 1999.

[59] T. Koopmans, Über die zuordnung von wellenfunktionen und eigenwerten zu den einzelnen elektronen eines atoms, Physica 1 (1934) 104-113.

[60] R. G. Pearson, Absolute electronegativity and hardness: applications to organic chemistry, J. Org. Chem. 54 (1989) 1423-1430.

34

[61] R. G. Parr, L. V. Szentpály, S. Liu, Electrophilicity index, J. Am. Chem. Soc. 121 (1999) 1922-1924.

[62] P. K. Chattaraj, U. Sarkar, D. R. Roy, Electrophilicity Index. Chem. Rev. 106 (2006) 2065-2091.

[63] R. G. Parr, P. K. Chattaraj, Principle of maximum hardness, J. Am. Chem. Soc. 113(5) (1991) 1854-1855.

[64] P Prasad, D. J. Williams, Introduction to Nonlinear Optical Effects in Molecules and Polymers; John Wiley & Sons: New York, 1991.

[65] S. Dhanuskodi, T. C. S. Girisun, N. Smijesh, R. Philip, Two-photon absorption and optical limiting in tristhiourea cadmium sulphate, Chem. Phys. Lett. 486 (2010) 80-83.

[66] R. K. Pandey, C. S. S. Sandeep, R. Philip, V. Lakshminarayanan, Enhanced optical nonlinearity of polyaniline-porphyrin nanocomposite, J. Phys. Chem. C 113(20) (2009) 8630-8634.

[67] A. J. Kiran, D. Udayakumar, K. Chandrasekharan, A. V. Ahdikari, H. D. Shashikala, R. Philip, Nonlinear Optical Studies of a Newly Synthesized Copolymer Containing Oxadiazole and Substituted Thiophenes, Opt. Commun. 271 (2007) 236-240.

TABLE CAPTIONS

Table 1: Optimized geometric parameters of UNMH.

Table 2: Experimental FT-IR, FT-Raman and theoretical wavenumbers in (cm^{-1}), IR and Raman intensities, vibrational assignments and PED contributions of UNMH by NCA based on SQM force field calculations.

Table 3: Calculated quantum chemical molecular orbital properties.

Table 4: Calculated electronic absorption spectral data of UNMH by TD-DFT/B3LYP/cc-pVTZ method.

FIGURE CAPTIONS

Figure 1:(a) Solubility curve of UNMH. (b) Photograph of as-grown single crystals of

UNMH.

Figure 2:(a) Optimized structure of UNMH molecule. (b) and (c) two different views of
the molecule.
Figure 3:(a) Experimental FT-IR and (b) Simulated IR spectra of UNMH.

Figure 4:(a) Experimental FT-Raman and (b) Simulated Raman spectra of UNMH.

Figure 5:(a) Molecular orbitals. (b) Computed electrostatic potential on the molecular

surface of UNMH.

Figure 6:(a) Solid state UV-Vis-NIR and simulated UV-Vis-NIR spectra for (b) gas (c) water
phases of UNMH.
Figure 7: (a) Open-aperture Z-scan curve. (b) Optical limiting curve of UNMH.

TABLES

Table 1: Optimized geometric parameters of UNMH.

Bond lengths	B3LYP (Å)	XRD[a] (Å)	Bond Angles	B3LYP (°)	XRD[a] (°)	Dihedral angles	B3LYP (°)	XRD[a] (°)
C_1-C_2	1.389	1.386	$C_1-C_2-C_3$	121.3	121.2	$C_1-C_2-C_3-C_4$	-0.1	0.0
C_2-C_3	1.400	1.393	$C_2-C_3-C_4$	120.3	120.8	$C_2-C_3-C_4-C_5$	0.2	-1.5
C_3-C_4	1.384	1.377	$C_3-C_4-C_5$	118.3	118.0	$C_3-C_4-C_5-C_6$	-0.1	1.4
C_4-C_5	1.395	1.398	$C_4-C_5-C_6$	121.5	121.2	$C_4-C_5-C_6-C_7$	-179.1	179.1
C_5-C_6	1.394	1.386	$C_5-C_6-C_7$	111.9	112.0	$C_5-C_6-C_7-N_8$	-115.8	-111.5
C_6-C_7	1.518	1.517	$C_6-C_7-N_8$	115.0	114.0	$C_6-C_7-N_8-C_9$	102.3	105.9
C_7-N_8	1.443	1.438	$C_7-N_8-C_9$	114.4	112.7	$C_7-N_8-C_9-N_{10}$	1.2	4.8
N_8-C_9	1.378	1.350	$N_8-C_9-N_{10}$	105.9	108.8	$N_8-C_9-N_{10}-C_{11}$	8.8	-1.2
C_9-N_{10}	1.389	1.355	$C_9-N_{10}-C_{11}$	113.3	113.1	$C_6-C_7-C_{11}-C_{12}$	8.3	1.9
$N_{10}-C_{11}$	1.438	1.434	$C_7-C_{11}-C_{12}$	105.1	105.3	$N_{10}-C_{11}-C_{12}=O_{13}$	-78.1	-72.5
$C_{11}-C_{12}$	1.548	1.540	$C_{11}-C_{12}=O_{13}$	125.2	123.3	$C_5-C_{12}-C_{11}-O_{14}$	-128.1	-124.9
$C_{12}=O_{13}$	1.218	1.209	$C_{12}-C_{11}-O_{14}$	113.6	111.9	$C_7-N_8-C_9=O_{15}$	-177.8	-174.5
$C_{11}-O_{14}$	1.396	1.397	$N_8-C_9=O_{15}$	127.4	125.8	$C_1-C_6-C_7-O_{16}$	-63.0	-59.0
$C_9=O_{15}$	1.209	1.236	$C_6-C_7-O_{16}$	108.9	109.0	$C_7-C_6-C_1-H_{17}$	-0.2	0.1
C_7-O_{16}	1.397	1.406	$C_6-C_1-H_{17}$	121.1	120.5	$H_{17}-C_1-C_2-H_{18}$	-0.6	-1.3
C_1-H_{17}	1.082	0.986	$C_1-C_2-H_{18}$	119.5	119.1	$C_5-C_4-C_3-H_{19}$	-179.9	176.9
C_2-H_{18}	1.082	0.958	$C_4-C_3-H_{19}$	120.2	119.7	$C_6-C_5-C_4-H_{20}$	179.9	179.5
C_3-H_{19}	1.081	0.966	$C_5-C_4-H_{20}$	120.0	120.9	$C_7-C_{11}-O_{14}-H_{21}$	175.9	-139.8
C_4-H_{20}	1.081	0.960	$C_{11}-O_{14}-H_{21}$	108.3	114.1	$C_6-C_7-O_{16}-H_{22}$	-143.4	178.1
$O_{14}-H_{21}$	0.980	0.902	$C_7-O_{16}-H_{22}$	107.2	107.9	$O_{15}=C_9-N_{10}-H_{23}$	-16.4	0.0
$O_{16}-H_{22}$	0.969	0.914	$C_9-N_{10}-H_{23}$	120.2	125.4	$C_{11}-C_7-N_8-H_{24}$	179.8	177.0
$N_{10}-H_{23}$	1.007	0.893	$C_7-N_8-H_{24}$	124.0	121.3	$O_{14}-H_{21}\cdots O_{25}-H_{26}$	43.1	-35.1
N_8-H_{24}	1.004	0.935	$O_{14}-H_{21}\cdots O_{25}$	155.3	88.3	$O_{25}-H_{26}\cdots O_{13}-C_{12}$	-1.7	153.9
$H_{21}\cdots O_{25}$	1.813	4.579	$O_{25}-H_{26}\cdots O_{13}$	149.9	115.7	$O_{13}\cdots H_{26}-O_{25}\cdots H_{21}$	-26.9	17.0
$O_{25}-H_{26}$	0.977	0.889	$C_{12}-O_{13}\cdots H_{26}$	114.7	86.0	$C_4-C_5-C_{12}-C_{11}$	-175.4	-177.9
$O_{25}-H_{27}$	0.960	0.899	$C_5-C_{12}-C_{11}$	107.5	107.9	$C_2-C_1-C_6-C_7$	179.0	179.6
C_5-C_{12}	1.466	1.465	$C_{11}-C_7-C_6$	103.9	104.0	$C_4-C_5-C_{12}=O_{13}$	3.9	2.0
C_7-C_{11}	1.576	1.574	$C_6-C_5-C_{12}$	110.8	110.8	$H_{22}-O_{16}-C_7-N_8$	87.3	50.8
C_1-C_6	1.388	1.386	$N_{10}-C_{11}-C_7$	102.6	102.3	$H_{21}-O_{14}-C_{11}-C_{12}$	-67.0	-21.7
			$C_{11}-C_7-N_8$	101.8	102.7	$H_{21}-O_{14}-C_{11}-N_{10}$	61.0	104.9
			$H_{26}-O_{25}-H_{27}$	107.2	108.3	$O_{14}-C_{11}-C_7-O_{16}$	12.4	5.0
						$C_5-C_{12}-C_{11}-N_{10}$	101.1	107.4
						$C_{12}-C_{11}-N_{10}-C_9$	-125.5	-114.3
						$C_1-C_6-C_7-N_8$	65.3	67.2

Hydrogen bonding geometry in UNMH				
X-H⋯Y	X-H length (Å)	H⋯Y length (Å)	X⋯Y length (Å)	X-H⋯Y angle (°)
$O_{16}-H_{22}\cdots O_{14}$	0.969	2.055	2.613	114.7
$O_{25}-H_{26}\cdots O_{13}$	0.977	1.857	2.747	149.9
$O_{14}-H_{21}\cdots O_{25}$	0.980	1.813	2.734	155.3

[a] UmaDevi, T.; Lawrence, N.; RameshBabu, R.; Selvanayagam, S.; Helen Stoeckli-Evans; Ramamurthi, K. Journal of Crystal Growth **2009**, 311, 3485-3490.

Table 2: Experimental FT-IR, FT-Raman and theoretical wavenumbers in (cm^{-1}), IR and Raman intensities, vibrational assignments and PED contributions of UNMH by NCA based on SQM Force field calculations.

Experimental		Theoretical	I_{IR}[a]	I_{Raman}[b]	Characterization of normal modes with PED
FT-IR	FT-Raman	Scaled	(km/mol)	(a.u)	(%)
3656 vw		3720	11.71	4.62	υ_{as}(OH$_{water}$) (100)
3571 ms		3574	9.06	2.77	υ(O$_{16}$H$_{22}$) (100)
3502 ms	3502 vw	3521	5.78	3.46	υ(N$_8$H$_{24}$) (100)
3467 w		3483	13.53	3.52	υ(N$_{10}$H$_{23}$) (99)
3431 w		3410	100	3.44	υ_s(OH$_{water}$) (97)
3310 vs	3308 vw	3321	29.67	12.44	υ(O$_{14}$H$_{21}$) (97)
3175 vs					υ(CH)
3096 vs	3094 vw	3073	1.40	16.99	υ(CH) (99)
	3082 vw	3065	1.01	6.00	υ(CH) (99)
	3070 vw	3058	0.52	6.46	υ(CH) (99)
		3046	0.09	3.38	υ(CH) (99)
1726 vs	1726 vs	1743	89.87	2.31	υ(C$_9$=O$_{15}$) (75), υ(CN) (11)
1683 vs	1683 vw	1683	22.73	21.15	υ(C$_{12}$=O$_{13}$) (71), γ(HOH) (10), υ(CC)$_{R2}$ (8)
1647 ms	1657 vw	1626	15.16	1.41	γ(HOH) (53), υ(CC)$_{R1}$ (19), β(CH) (8)
1619 s	1605 w	1612	28.99	24.39	υ(CC)$_{R1}$ (42), β(CH) (20), γ(HOH) (16), υ(C$_{12}$=O$_{13}$) (11), β(CCC)$_{R1}$ (7)
1603 s	1590 w	1603	0.18	9.15	υ(CC)$_{R1}$ (60), β(CH) (22), β(CCC)$_{R1}$ (11)
1523 vw	1526 vw	1524	0.98	0.06	β(CH) (66), υ(CC)$_{R1}$ (28)
		1516	0.86	1.21	β(CH) (65), υ(CC)$_{R1}$ (28)
1469 ms	1469 vw	1469	5.68	1.35	β(COH) (55), β(CN$_{10}$H$_{23}$) (14), υ(O$_{13}$···H$_{21}$) (10)
1418s	1415 vw	1415	15.04	0.55	β(COH) (46), β(CN$_8$H$_{24}$) (16), υ(CC)$_{R2}$ (13), β(C$_7$O$_{16}$) (5)
1395 s		1353	2.99	1.06	β(CN$_{10}$H$_{23}$) (54), β(CN$_8$H$_{24}$) (14), υ(CN) (11), β(COH) (8)
		1349	2.35	1.39	β(CN$_8$H$_{24}$) (24), β(CH) (23), υ(CC)$_{R1}$ (15), β(COH) (14), υ(CN) (5)
1343 ms	1334 vw	1340	5.72	2.13	β(CH) (24), υ(CC)$_{R1}$ (22), β(CN$_8$H$_{24}$) (19), β(COH) (14)
		1314	6.36	2.72	υ(CC)$_{R2}$ (39), β(CH) (24), υ(CN) (15), β(NC=O) (6), β(COH) (6)
1294 s	1295 vw	1295	13.64	0.99	υ(CN) (31), υ(CC)$_{R2}$ (26), β(CH) (19), β(NC=O) (11)
1261ms	1256 vw	1246	3.41	5.44	υ(CC)$_{R2}$ (52), β(CH) (17), β(COH) (10)
1218 s	1223 vw	1217	5.94	2.93	υ(CC)$_{R2}$ (38), β(CCC)$_{R1}$ (23), β(CH) (9), β(COH) (8), υ(CN) (7)
1184 s	1182 vw	1194	0.09	3.87	υ(CC)$_{R2}$ (65), β(CH) (30)
1150 s	1165 vw	1168	8.67	2.81	υ(CC)$_{R2}$ (27), υ(CN) (14), υ(C-O) (14), β(CH) (9), β(C$_{11}$O$_{14}$) (8), β(COH) (6)
1137 s	1132 vw	1143	1.56	6.96	υ(CC)$_{R2}$ (38), β(CH) (24), β(CCC)$_{R1}$ (12), υ(C-O) (8)
1113 vs	1114 vw	1099	3.35	0.97	υ(C-O) (42), υ(CN) (14), Γ(CCCC)$_{R2}$ (7), β(C$_7$O$_{16}$) (7), β(C$_{11}$O$_{14}$) (5)
1084 s	1084 vw	1092	1.89	3.12	υ(CC)$_{R2}$ (24), υ(CN) (23), β(CCC)$_{R1}$ (17), β(C$_7$O$_{16}$) (8), β(C$_{11}$O$_{14}$) (6)
1048 w	1051 vw	1070	26.58	2.95	υ(C-O) (53), υ(CN) (21)
1027 w	1028 vw	1027	1.47	16.1	υ(CC)$_{R2}$ (72), β(CH) (17)
1010 w	1013 w	1010	4.30	0.45	υ(CN) (35), υ(CC)$_{R2}$ (19), β(CN$_{10}$H$_{23}$) (10), β(C$_{11}$O$_{14}$) (10), β(CN$_8$H$_{24}$) (7)
		1000	0.02	0.02	ω_{out}(CH) (85), β(CCC)$_{PUCK}$(13)
	974 vw	979	3.50	6.59	υ(CN) (47), υ(CC)$_{R2}$ (21)
964 w		969	0.21	0.01	ω_{out} (CH) (90), R$_{br}$(CCCC)$_{R1}$ (9)
933 s	941 w	919	1.77	0.56	β(CCC)$_{R1}$ (24), υ(CC)$_{R2}$ (21), β(CC=O) (15), β(C$_7$O$_{16}$) (11), β(C$_{11}$O$_{14}$) (8)
904 s	909 vw	914	11.03	4.04	υ(CC)$_{R2}$ (41), υ(C-O) (13), β(CC=O) (11), β(C$_7$O$_{16}$) (8), υ(CN) (7), β(C$_{11}$O$_{14}$) (6)
880 w		897	0.44	0.32	ω_{out}(CH) (62), β(CCC)$_{PUCK}$(21)
		835	0.11	0.17	β(CCC)$_{PUCK}$(32), ω_{out}(CH) (27), ω(C$_{12}$=O$_{13}$) (18), Γ(CCCC)$_{R2}$ (11)
810 ms	811 vw	791	0.76	0.61	ω_{out}(CH) (40), β(CCC)$_{PUCK}$(22), ω(C$_{12}$=O$_{13}$) (10)
781 ms	790 vw	780	20.33	2.32	τ(O···H···O···H) (27), τ(C$_{11}$O$_{14}$H$_{21}$···O$_{25}$) (23), β (O···H···O) (15), Γ(C$_{11}$O$_{14}$) (15), τ(O$_{25}$H$_{26}$) (10)
		760	1.89	1.69	ω(C$_9$=O$_{15}$) (38), ω_{out}(CH) (17), Γ(CNC)$_{R3}$

					(14),
751 vs	750 vw	750	0.81	1.28	$\omega(C_9=O_{15})$ (45), $\Gamma(CNC)_{R3}$ (15), $\omega_{out}(CH)$ (5)
		737	2.44	3.77	$\beta(CCC)_{R1}$ (41), $\beta(CC=O)$ (13), $\upsilon(CC)_{R2}$ (10)
727 s	728 vw	731	5.25	3.94	$\omega_{out}(CH)$ (40), $\omega(C_{12}=O_{13})$ (12), $\beta(CCC)_{PUCK}$(9), $\beta(CCC)_{R1}$ (6), $\upsilon(CC)_{R2}$ (6)
671 s	674 vw	688	2.05	4.74	$\beta(CCC)_{R1}$ (48), $\beta(C_7O_{16})$ (8), $\beta(NC=O)$ (8), $\upsilon(CC)_{R2}$ (7)
655 s	656 vw	651	1.01	4.16	$\beta(NC=O)$ (18), $\beta(C_{11}O_{14})$ (17), $\beta(CCC)_{PUCK}$(11), $\beta(C_7O_{16})$ (7), $\omega(C_{12}=O_{13})$ (6), $\beta(CCC)_{R1}$ (5)
		605	0.47	4.92	$\beta(CCC)_{PUCK}$(17), $\upsilon(C-O)$ (15), $\omega_{out}(CH)$ (14), $\Gamma(CCCC)_{R1}$ (12), $\beta(C_7O_{16})$ (9)
593 ms	596 vw	578	13.70	1.72	$\tau(O_{14}H_{21})$ (33), $\Gamma(C_{11}O_{14})$ (24), $\tau(O\cdots H\cdots O\cdots H)$ (12), $\upsilon(O_{13}\cdots H_{21})$ (10), $\tau(O_{25}H_{26})$ (10)
546 s	554 vw	543	0.53	7.46	$\upsilon(CC)_{R2}$ (22), $\delta(CCC)_{R1}$ (20), $\beta(CCC)_{ITR}$ (19), $\beta(CCC)_{R2}$ (11), $\beta(CC=O)$ (10)
528 ms	534 w	537	0.65	13.14	$\upsilon(CN)$ (15), $\delta(C_{11}O_{14})$ (13), $\tau(O_{14}H_{21})$ (9), $\delta(CCC)_{R1}$ (7), $\upsilon(CC)_{R2}$ (7), $\tau(CNC)_{R3}$ (6)
497 s	506 vw	519	1.58	1.04	$\Gamma(CCCC)_{R1}$ (29), $\delta(C_7O_{16})$ (11), $\omega_{out}(CH)$ (8), $\omega(N_{10}H_{23})$ (6)
		475	9.7	0.88	$\omega(N_{10}H_{23})$ (29), $\tau(O_{14}H_{21})$ (18), $\tau(C_{11}O_{14})$ (14), $\upsilon(O_{13}\cdots H_{21})$ (7), $\beta(NC=O)$ (7)
454 vs	452 vw	453	2.04	0.58	$\Gamma(CCCC)_{R1}$ (64), $\omega_{out}(CH)$ (7)
424 ms	433 vw	446	12.96	1.41	$\tau(O\cdots H\cdots O\cdots H)$ (29), $\delta(O\cdots H)$ (14), $\Gamma(CCCC)_{R1}$ (12), $\beta(NC=O)$ (9), $\tau(O_{25}H_{26})$ (7)
419 ms	410 vw	418	1.80	1.51	$\tau(O\cdots H\cdots O\cdots H)$ (25), $\omega(N_{10}H_{23})$ (14), $\tau(O_{25}H_{26})$ (10), $\delta(O\cdots H)$ (9), $\beta(NC=O)$ (8), $\upsilon(CN)$ (6)
		398	9.47	2.69	$\tau(C_7O_{16})$ (49), $\delta(C_7O_{16})$ (9), $\tau(O_{14}H_{21})$ (7), $\omega(N_{10}H_{23})$ (6), $\tau(C_{11}O_{14})$ (6)
	388 vw	379	1.62	10.91	$\upsilon(CC)_{R2}$ (23), $\delta(C_7O_{16})$ (20), $\delta(CCC)_{R1}$ (9), $\tau(CNC)_{R3}$ (6), $\beta(CCC)_{ITR}$ (6)
	355 vw	375	2.61	3.55	$\delta(C_{11}O_{14})$ (27), $\omega(N_8H_{24})$ (18), $\delta(C_7O_{16})$ (13), $\upsilon(O\cdots H)$ (10)
	336 vw	342	2.40	4.43	$\tau(CCCC)_{R1}$ (17), $\upsilon(O_{13}\cdots H_{21})$ (14), $\omega(N_{10}H_{23})$ (13), $\omega(N_8H_{24})$ (12), $\delta(C_7O_{16})$ (7), $\upsilon(O\cdots H)$ (6)
	317 vw	321	2.67	2.90	$\upsilon(O_{13}\cdots H_{21})$ (32), $\delta(C_{11}O_{14})$ (14), $\beta(CC=O)$ (14), $\upsilon(O\cdots H)$ (10), $\tau(CCCC)_{R1}$ (8)
	301 vw	307	2.60	5.22	$\delta(C_7O_{16})$ (37), $\upsilon(O\cdots H)$ (15), $\tau(C_7O_{16})$ (14), $\delta(C_{11}O_{14})$ (10)
		286	3.35	3.42	$\omega(N_8H_{24})$ (39), $\tau(CCCC)_{R1}$ (11), $\tau(C_7O_{16})$ (9)
	256 vw	257	12.62	6.48	$\tau(O_{25}H_{26})$ (67), $\delta(O\cdots H)$ (8)
	239 vw	244	0.36	1.14	$\beta(CCC)_{ITR}$ (16), $\upsilon(CC)_{R2}$(15), $\delta(C_7O_{16})$ (13), $\delta(CCC)_{R1}$ (13), $\delta(C_{11}O_{14})$ (7), $\tau(C_7O_{16})$ (7)
	209 vw	199	1.55	9.16	$\tau(CNC)_{R3}$ (25), $\delta(C_{11}O_{14})$ (21), $\omega(C_{12}O_{13})$ (12), $\tau(C_7O_{16})$ (7), $\omega(N_{10}H_{23})$ (7), $\delta(C_7O_{16})$ (5)
	183w	167	0.54	0.42	$\upsilon(O\cdots H)$ (56), $\delta(C_{11}O_{14})$ (11), $\upsilon(O_{13}\cdots H_{21})$ (7), $\tau(O_{25}H_{26})$ (6)
		145	0.07	18.88	$\omega(N_8H_{24})$ (24), $\tau(CNC)_{R3}$ (24), $BTFLY_{R1, R2}$ (10), $\delta(C_7O_{16})$ (6), $\tau(CCCC)_{R2}$ (6), $\omega(C_{12}O_{13})$ (5)
		136	1.49	1.55	$\upsilon(O\cdots H)$ (56), $\beta(CC=O)$ (8), $\tau(C_{11}O_{14})$ (8)
		110	0.26	24.77	$\tau(CNC)_{R3}$ (32), $\omega(N_8H_{24})$ (24), $\tau(CCCC)_{R2}$ (19), $\tau(CCCC)_{R1}$ (6)
		61	0.12	32.9	$\tau(CNC)_{R3}$ (51), $\omega(N_{10}H_{23})$ (19), $\tau(CCCC)_{R2}$ (12), $\omega(N_8H_{24})$ (11)
		31	0.59	54.53	$\tau(CNC)_{R3}$ (38), $\omega(N_8H_{24})$ (29), $\tau(C_{11}O_{14})$ (7), $\tau(O_{25}H_{26})$ (6)
		25	0.11	100	$\tau(CNC)_{R3}$ (39), $\omega(N_8H_{24})$ (30), $\tau(C_{11}O_{14})$ (9), $\tau(CCCC)_{R2}$ (6)

υ: stretching, γ: scissoring, ω: wagging, τ: torsion, Γ: twisting, β: in-plane bending, δ: out- of- plane bending, R_{br}: ring breathing, BTFLY: butterfly mode, ITR: inter-ring, R1: ring1-benzene ring, R2: ring2- fused cyclopentanone ring, R3: ring3- substituted urea moiety ring, in: in-plane, out: out-of-plane, s: symmetric, as: antisymmetric, vs: very strong, s: strong, ms: medium strong, vw: very weak, w: weak.

[a] Relative IR absorption intensities normalized with the highest peak absorption equal to 100.

[b] Relative Raman intensities normalized to 100.

Table 3: Calculated quantum chemical molecular orbital properties.

Parameters	B3LYP/cc-pVTZ
HOMO energy, E_{HOMO} (eV)	-7.1024
LUMO energy, E_{LUMO} (eV)	-2.4259
HOMO- LUMO energy gap, ΔE_{GAP} (eV)	4.6765
Ionisation potential, IP (eV)	7.1024
Electron affinity, EA (eV)	2.4259
Electronegativity, χ (eV)	4.7642
Chemical hardness, η (eV)	2.3383
Global softness, S (eV)$^{-1}$	0.2138
Chemical potential, μ (eV)	-4.7642
Electrophilicity index, ω (eV)	4.8534
Total energy change, ΔE_{T} (eV)	-0.5846
Overall energy balance, ΔE (eV)	-4.6765
SCF energy (eV)	-23757.6123

Table 4: Calculated electronic absorption spectral data of UNMH by TD-DFT/B3LYP/cc-pVTZ method.

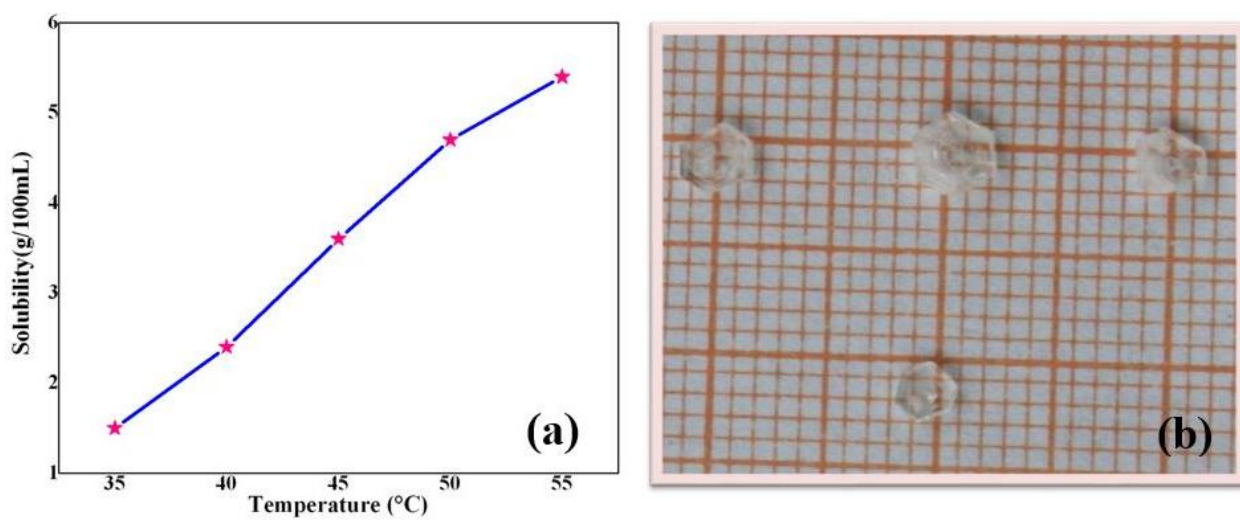| Phase	Excited State, S	Electronic contributions (%)	Wavelength (nm)	Excitation energies (eV)	Oscillator Strengths, f	Assignment
Gas	S1(H→ L)	79.1	346.57	3.5774	0.0039	n→π*
	S2(H-1 → L)	89.4	300.94	4.1199	0.0224	n→π*
	S3(H-2→ L)	92.8	286.56	4.3267	0.0046	n→π*
Water	S1(H→ L)	86.7	335.73	3.6930	0.0038	n→π*
	S2(H-1 → L)	90.9	292.10	4.2445	0.0404	n→π*
	S3(H-3→ L)	73.2	268.04	4.6255	0.0281	n→π*

H:HOMO, L:LUMO.

FIGURES

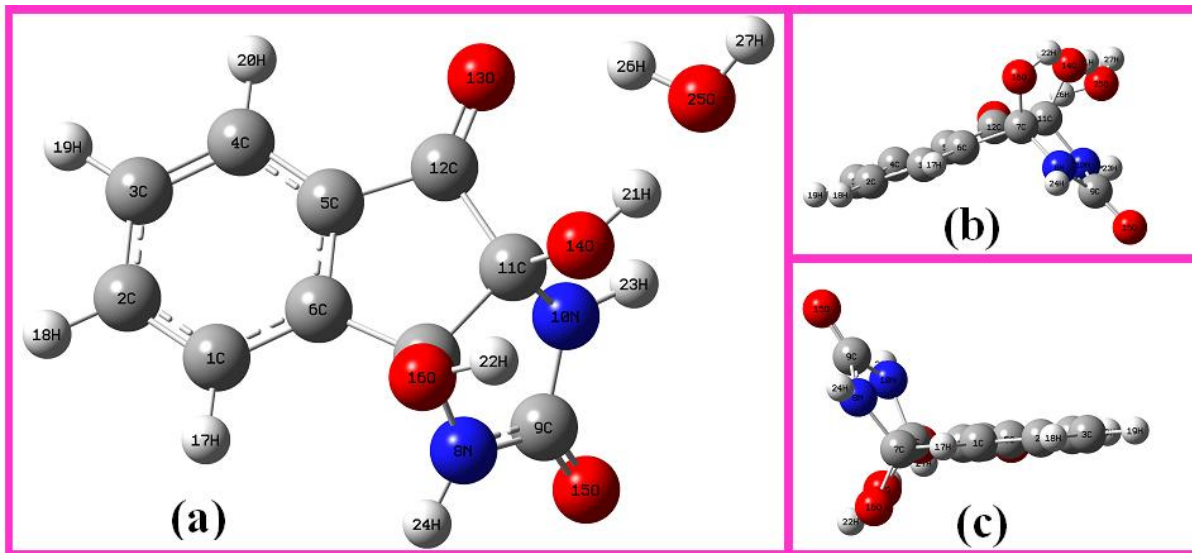**Fig. 1.** (a) Solubility curve of UNMH. (b) Photograph of as-grown single crystals of UNMH.

Fig.2. (a) Optimized structure of UNMH molecule. (b) and (c) two different views of the molecule.
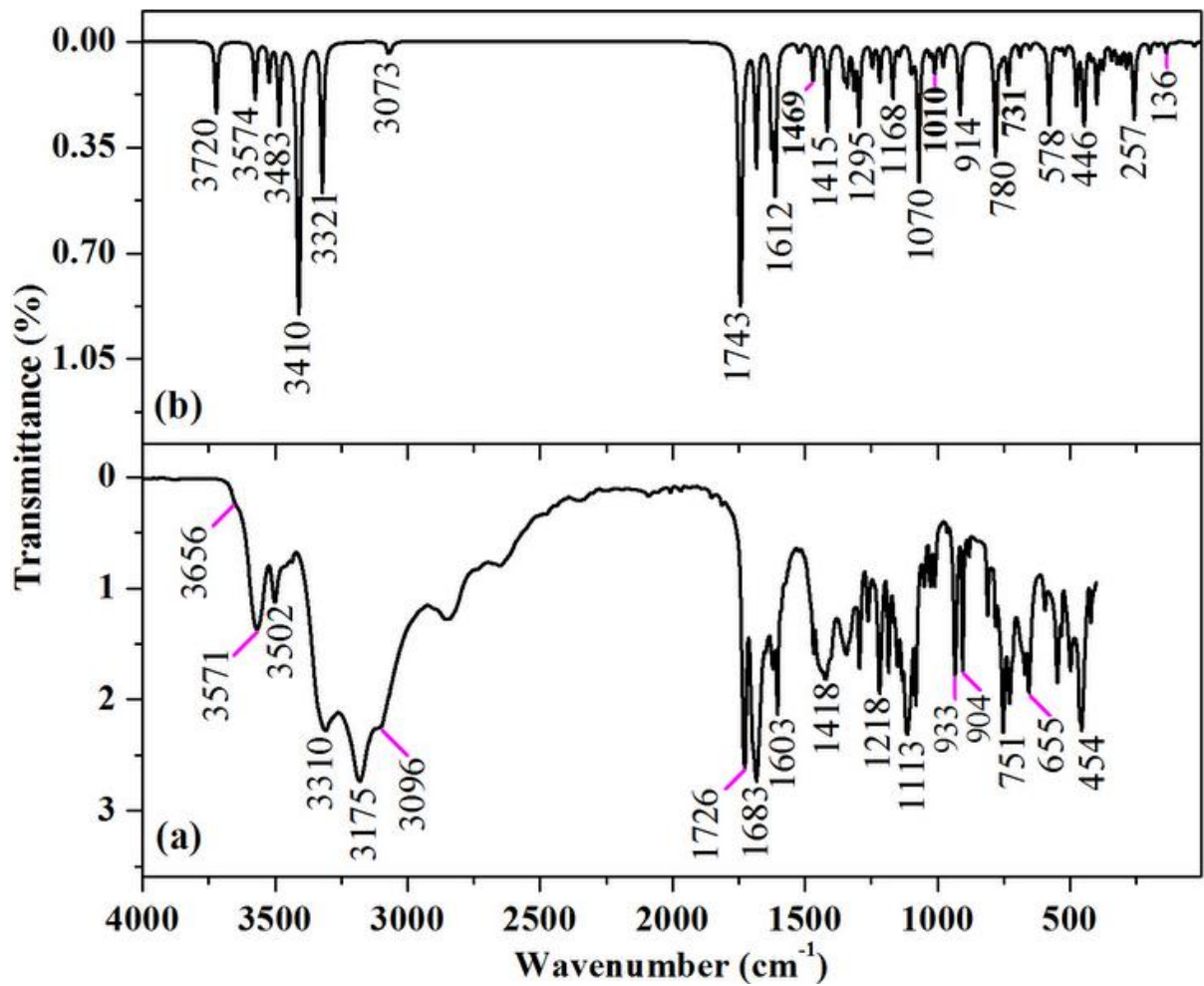
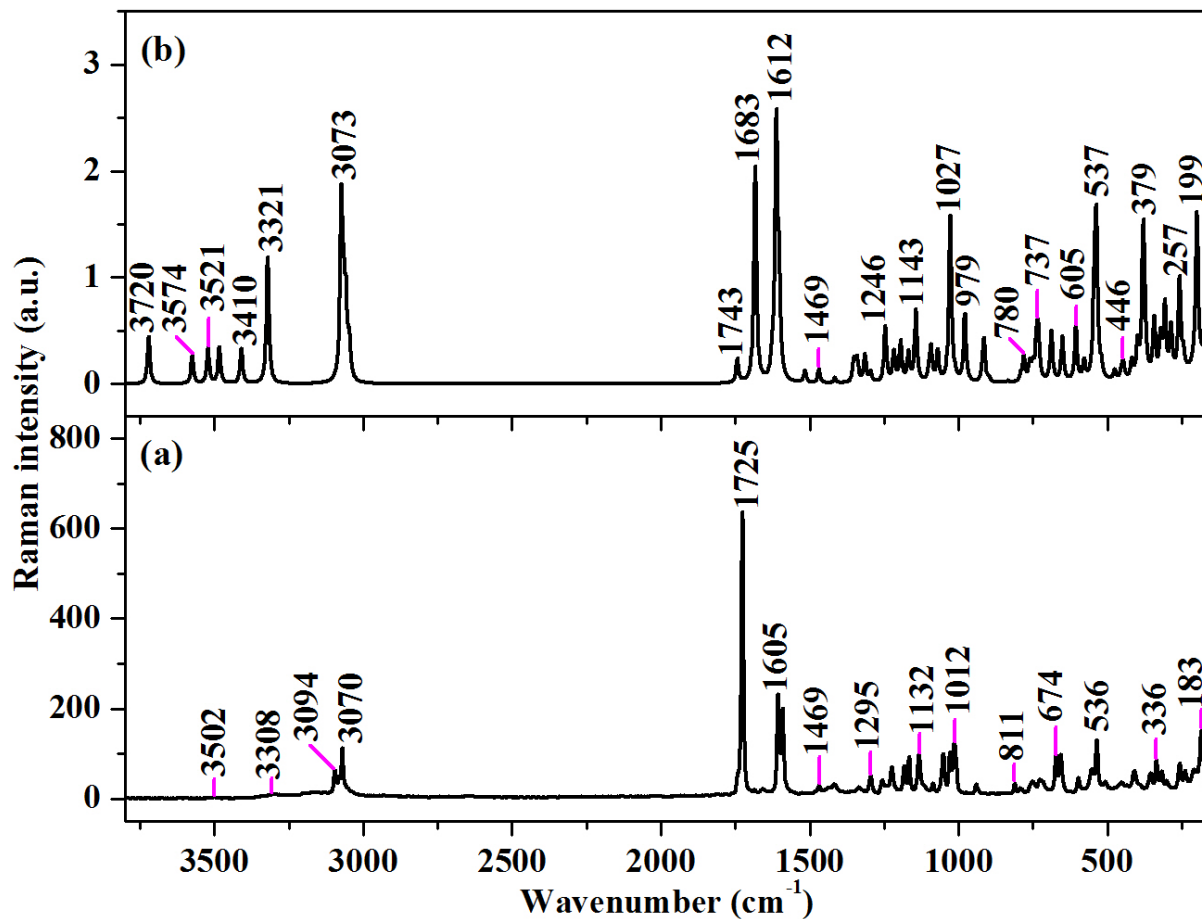**Fig. 3**. (a) Experimental FT-IR and (b) Simulated IR spectra of UNMH.

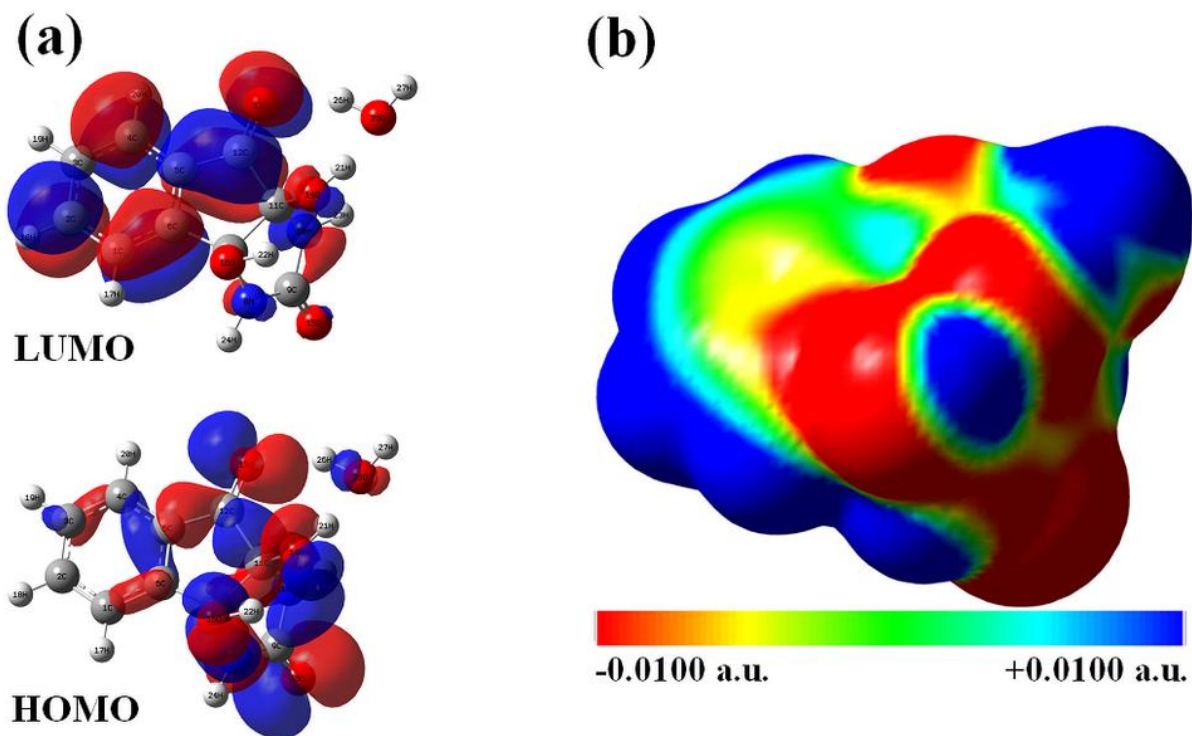**Fig. 4**. (a) Experimental FT-Raman and (b) Simulated Raman spectra of UNMH.

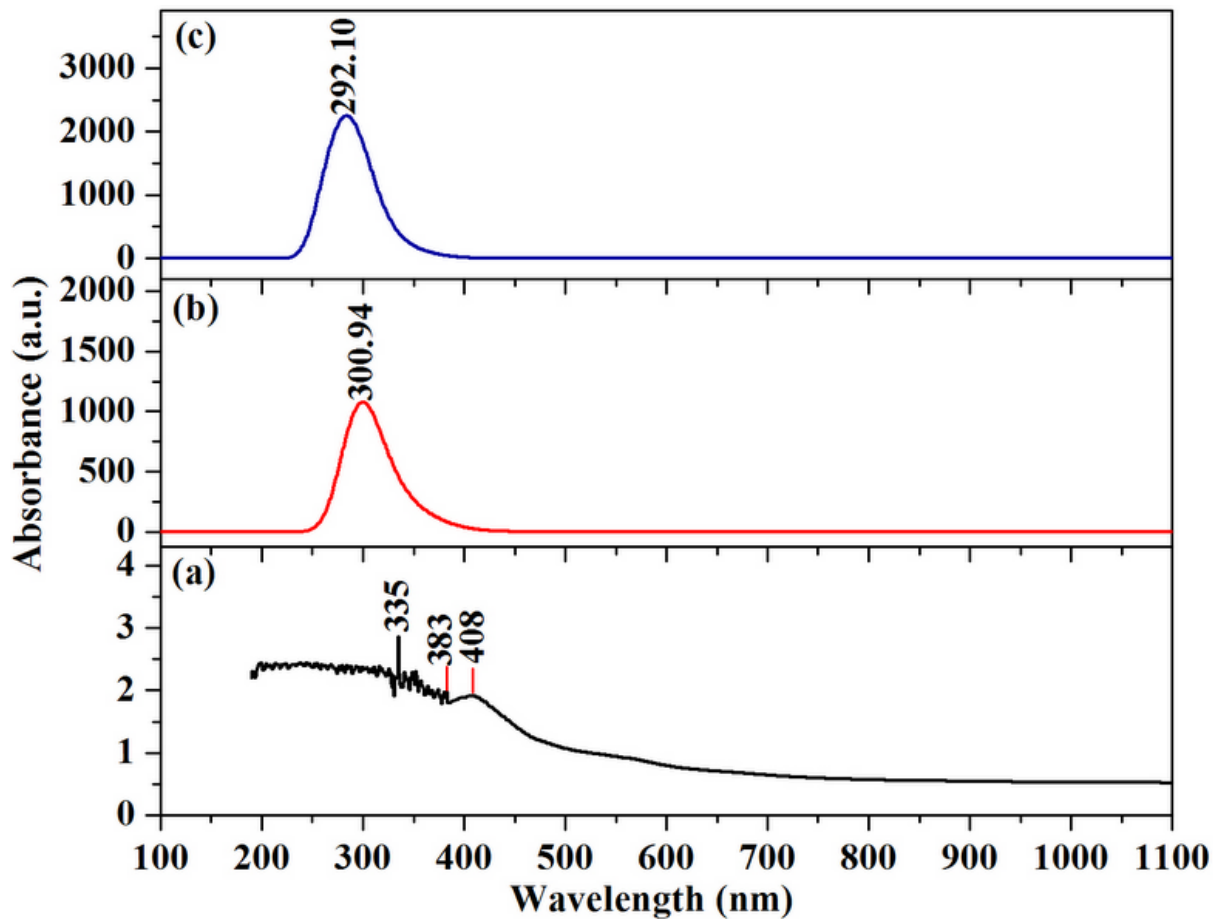**Fig. 5**. (a) HOMO-LUMO plot. (b) Computed electrostatic potential on the molecular surface of UNMH.

Fig. 6. (a) Solid state UV-Vis-NIR and simulated UV-Vis-NIR spectra for (b) gas and (c) water phases of UNMH.
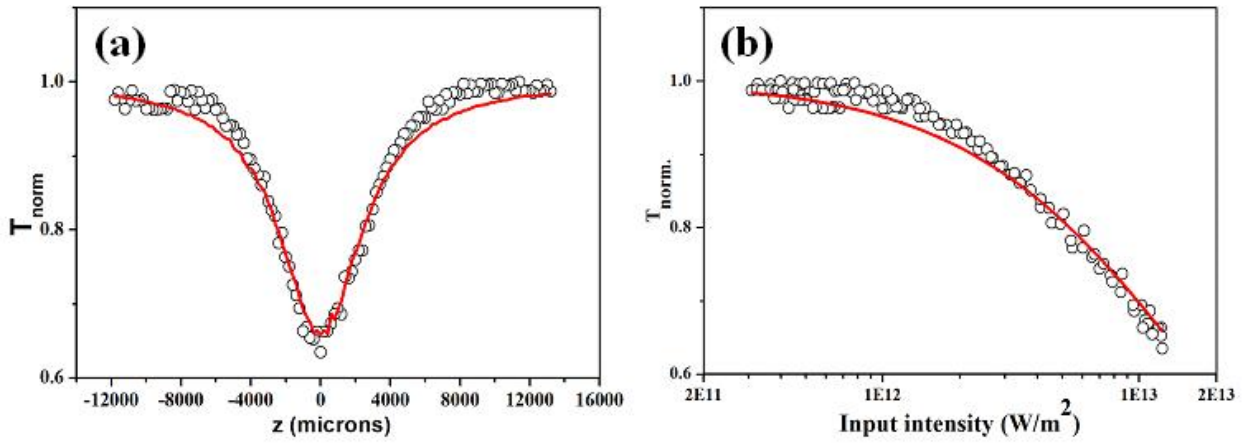
Fig. 7. (a) Open-aperture Z-scan curve. (b) Optical limiting curve of UNMH.

Table 1: Optimized geometric parameters of UNMH.

Bond lengths	B3LYP (Å)	XRD[a] (Å)	Bond Angles	B3LYP (°)	XRD[a] (°)	Dihedral angles	B3LYP (°)	XRD[a] (°)
C_1-C_2	1.389	1.386	C_1-C_2-C_3	121.3	121.2	C_1-C_2-C_3-C_4	-0.1	0.0
C_2-C_3	1.400	1.393	C_2-C_3-C_4	120.3	120.8	C_2-C_3-C_4-C_5	0.2	-1.5
C_3-C_4	1.384	1.377	C_3-C_4-C_5	118.3	118.0	C_3-C_4-C_5-C_6	-0.1	1.4
C_4-C_5	1.395	1.398	C_4-C_5-C_6	121.5	121.2	C_4-C_5-C_6-C_7	-179.1	179.1
C_5-C_6	1.394	1.386	C_5-C_6-C_7	111.9	112.0	C_5-C_6-C_7-N_8	-115.8	-111.5
C_6-C_7	1.518	1.517	C_6-C_7-N_8	115.0	114.0	C_6-C_7-N_8-C_9	102.3	105.9
C_7-N_8	1.443	1.438	C_7-N_8-C_9	114.4	112.7	C_7-N_8-C_9-N_{10}	1.2	4.8
N_8-C_9	1.378	1.350	N_8-C_9-N_{10}	105.9	108.8	N_8-C_9-N_{10}-C_{11}	8.8	-1.2
C_9-N_{10}	1.389	1.355	C_9-N_{10}-C_{11}	113.3	113.1	C_6-C_7-C_{11}-C_{12}	8.3	1.9
N_{10}-C_{11}	1.438	1.434	C_7-C_{11}-C_{12}	105.1	105.3	N_{10}-C_{11}-C_{12}=O_{13}	-78.1	-72.5
C_{11}-C_{12}	1.548	1.540	C_{11}-C_{12}=O_{13}	125.2	123.3	C_5-C_{12}-C_{11}-O_{14}	-128.1	-124.9
C_{12}=O_{13}	1.218	1.209	C_{12}-C_{11}-O_{14}	113.6	111.9	C_7-N_8-C_9=O_{15}	-177.8	-174.5
C_{11}-O_{14}	1.396	1.397	N_8-C_9=O_{15}	127.4	125.8	C_1-C_6-C_7-O_{16}	-63.0	-59.0
C_9=O_{15}	1.209	1.236	C_6-C_7-O_{16}	108.9	109.0	C_7-C_6-C_1-H_{17}	-0.2	0.1
C_7-O_{16}	1.397	1.406	C_6-C_1-H_{17}	121.1	120.5	H_{17}-C_1-C_2-H_{18}	-0.6	-1.3
C_1-H_{17}	1.082	0.986	C_1-C_2-H_{18}	119.5	119.1	C_5-C_4-C_3-H_{19}	-179.9	176.9
C_2-H_{18}	1.082	0.958	C_4-C_3-H_{19}	120.2	119.7	C_6-C_5-C_4-H_{20}	179.9	179.5
C_3-H_{19}	1.081	0.966	C_5-C_4-H_{20}	120.0	120.9	C_7-C_{11}-O_{14}-H_{21}	175.9	-139.8
C_4-H_{20}	1.081	0.960	C_{11}-O_{14}-H_{21}	108.3	114.1	C_6-C_7-O_{16}-H_{22}	-143.4	178.1
O_{14}-H_{21}	0.980	0.902	C_7-O_{16}-H_{22}	107.2	107.9	O_{15}=C_9-N_{10}-H_{23}	-16.4	0.0
O_{16}-H_{22}	0.969	0.914	C_9-N_{10}-H_{23}	120.2	125.4	C_{11}-C_7-N_8-H_{24}	179.8	177.0
N_{10}-H_{23}	1.007	0.893	C_7-N_8-H_{24}	124.0	121.3	O_{14}-H_{21}⋯O_{25}-H_{26}	43.1	-35.1
N_8-H_{24}	1.004	0.935	O_{14}-H_{21}⋯O_{25}	155.3	88.3	O_{25}-H_{26}⋯O_{13}-C_{12}	-1.7	153.9
H_{21}⋯O_{25}	1.813	4.579	O_{25}-H_{26}⋯O_{13}	149.9	115.7	O_{13}⋯H_{26}-O_{25}⋯H_{21}	-26.9	17.0
O_{25}-H_{26}	0.977	0.889	C_{12}-O_{13}⋯H_{26}	114.7	86.0	C_4-C_5-C_{12}-C_{11}	-175.4	-177.9
O_{25}-H_{27}	0.960	0.899	C_5-C_{12}-C_{11}	107.5	107.9	C_2-C_1-C_6-C_7	179.0	179.6
C_5-C_{12}	1.466	1.465	C_{11}-C_7-C_6	103.9	104.0	C_4-C_5-C_{12}=O_{13}	3.9	2.0
C_7-C_{11}	1.576	1.574	C_6-C_5-C_{12}	110.8	110.8	H_{22}-O_{16}-C_7-N_8	87.3	50.8
C_1-C_6	1.388	1.386	N_{10}-C_{11}-C_7	102.6	102.3	H_{21}-O_{14}-C_{11}-C_{12}	-67.0	-21.7
			C_{11}-C_7-N_8	101.8	102.7	H_{21}-O_{14}-C_{11}-N_{10}	61.0	104.9
			H_{26}-O_{25}-H_{27}	107.2	108.3	O_{14}-C_{11}-C_7-O_{16}	12.4	5.0
						C_5-C_{12}-C_{11}-N_{10}	101.1	107.4
						C_{12}-C_{11}-N_{10}-C_9	-125.5	-114.3
						C_1-C_6-C_7-N_8	65.3	67.2

Hydrogen bonding geometry in UNMH				
X-H⋯Y	X-H length (Å)	H⋯Y length (Å)	X⋯Y length (Å)	X-H⋯Y angle (°)
O_{16}-H_{22}⋯O_{14}	0.969	2.055	2.613	114.7
O_{25}-H_{26}⋯O_{13}	0.977	1.857	2.747	149.9
O_{14}-H_{21}⋯O_{25}	0.980	1.813	2.734	155.3

[a] UmaDevi, T.; Lawrence, N.; RameshBabu, R.; Selvanayagam, S.; Helen Stoeckli-Evans; Ramamurthi, K. Journal of Crystal Growth **2009**, 311, 3485-3490.

Table 2: Experimental FT-IR, FT-Raman and theoretical wavenumbers in (cm^{-1}), IR and Raman intensities, vibrational assignments and PED contributions of UNMH by NCA based on SQM force field calculations.

Experimental		Theoretical	I_{IR} [a]	I_{Raman} [b]	Characterization of normal modes with PED
FT-IR	FT-Raman	Scaled	(km/mol)	(a.u)	(%)
3656 vw		3720	11.71	4.62	υ_{as}(OH$_{water}$) (100)
3571 ms		3574	9.06	2.77	υ(O$_{16}$H$_{22}$) (100)
3502 ms	3502 vw	3521	5.78	3.46	υ(N$_8$H$_{24}$) (100)
3467 w		3483	13.53	3.52	υ(N$_{10}$H$_{23}$) (99)
3431 w		3410	100	3.44	υ_s(OH$_{water}$) (97)
3310 vs	3308 vw	3321	29.67	12.44	υ(O$_{14}$H$_{21}$) (97)
3175 vs					υ(CH)
3096 vs	3094 vw	3073	1.40	16.99	υ(CH) (99)
	3082 vw	3065	1.01	6.00	υ(CH) (99)
	3070 vw	3058	0.52	6.46	υ(CH) (99)
		3046	0.09	3.38	υ(CH) (99)
1726 vs	1726 vs	1743	89.87	2.31	υ(C$_9$=O$_{15}$) (75), υ(CN) (11)
1683 vs	1683 vw	1683	22.73	21.15	υ(C$_{12}$=O$_{13}$) (71), γ(HOH) (10), υ(CC)$_{R2}$ (8)
1647 ms	1657 vw	1626	15.16	1.41	γ(HOH) (53), υ(CC)$_{R1}$ (19), β(CH) (8)
1619 s	1605 w	1612	28.99	24.39	υ(CC)$_{R1}$ (42), β(CH) (20), γ(HOH) (16), υ(C$_{12}$=O$_{13}$) (11), β(CCC)$_{R1}$ (7)
1603 s	1590 w	1603	0.18	9.15	υ(CC)$_{R1}$ (60), β(CH) (22), β(CCC)$_{R1}$ (11)
1523 vw	1526 vw	1524	0.98	0.06	β(CH) (66), υ(CC)$_{R1}$ (28)
		1516	0.86	1.21	β(CH) (65), υ(CC)$_{R1}$ (28)
1469 ms	1469 vw	1469	5.68	1.35	β(COH) (55), β(CN$_{10}$H$_{23}$) (14), υ(O$_{13}\cdots$H$_{21}$) (10)
1418s	1415 vw	1415	15.04	0.55	β(COH) (46), β(CN$_8$H$_{24}$) (16), υ(CC)$_{R2}$ (13), β(C$_7$O$_{16}$) (5)
1395 s		1353	2.99	1.06	β(CN$_{10}$H$_{23}$) (54), β(CN$_8$H$_{24}$) (14), υ(CN) (11), β(COH) (8)
		1349	2.35	1.39	β(CN$_8$H$_{24}$) (24), β(CH) (23), υ(CC)$_{R1}$ (15), β(COH) (14), υ(CN) (5)
1343 ms	1334 vw	1340	5.72	2.13	β(CH) (24), υ(CC)$_{R1}$ (22), β(CN$_8$H$_{24}$) (19), β(COH) (14)
		1314	6.36	2.72	υ(CC)$_{R2}$ (39), β(CH) (24), υ(CN) (15), β(NC=O) (6), β(COH) (6)
1294 s	1295 vw	1295	13.64	0.99	υ(CN) (31), υ(CC)$_{R2}$ (26), β(CH) (19), β(NC=O) (11)
1261ms	1256 vw	1246	3.41	5.44	υ(CC)$_{R2}$ (52), β(CH) (17), β(COH) (10)
1218 s	1223 vw	1217	5.94	2.93	υ(CC)$_{R2}$ (38), β(CCC)$_{R1}$ (23), β(CH) (9), β(COH) (8), υ(CN) (7)
1184 s	1182 vw	1194	0.09	3.87	υ(CC)$_{R2}$ (65), β(CH) (30)
1150 s	1165 vw	1168	8.67	2.81	υ(CC)$_{R2}$ (27), υ(CN) (14), υ(C-O) (14), β(CH) (9), β(C$_{11}$O$_{14}$) (8), β(COH) (6)
1137 s	1132 vw	1143	1.56	6.96	υ(CC)$_{R2}$ (38), β(CH) (24), β(CCC)$_{R1}$ (12), υ(C-O) (8)
1113 vs	1114 vw	1099	3.35	0.97	υ(C-O) (42), υ(CN) (14), Γ(CCCC)$_{R2}$ (7), β(C$_7$O$_{16}$) (7), β(C$_{11}$O$_{14}$) (5)
1084 s	1084 vw	1092	1.89	3.12	υ(CC)$_{R2}$ (24), υ(CN) (23), β(CCC)$_{R1}$ (17), β(C$_7$O$_{16}$) (8), β(C$_{11}$O$_{14}$) (6)
1048 w	1051 vw	1070	26.58	2.95	υ(C-O) (53), υ(CN) (21)
1027 w	1028 vw	1027	1.47	16.1	υ(CC)$_{R2}$ (72), β(CH) (17)
1010 w	1013 w	1010	4.30	0.45	υ(CN) (35), υ(CC)$_{R2}$ (19), β(CN$_{10}$H$_{23}$) (10), β(C$_{11}$O$_{14}$) (10), β(CN$_8$H$_{24}$) (7)
		1000	0.02	0.02	ω_{out}(CH) (85), β(CCC)$_{PUCK}$(13)
	974 vw	979	3.50	6.59	υ(CN) (47), υ(CC)$_{R2}$ (21)
964 w		969	0.21	0.01	ω_{out} (CH) (90), R$_{br}$(CCCC)$_{R1}$ (9)
933 s	941 w	919	1.77	0.56	β(CCC)$_{R1}$ (24), υ(CC)$_{R2}$ (21), β(CC=O) (15), β(C$_7$O$_{16}$) (11), β(C$_{11}$O$_{14}$) (8)
904 s	909 vw	914	11.03	4.04	υ(CC)$_{R2}$ (41), υ(C-O) (13), β(CC=O) (11), β(C$_7$O$_{16}$) (8), υ(CN) (7), β(C$_{11}$O$_{14}$) (6)

880 w		897	0.44	0.32	ω_{out}(CH) (62), β(CCC)$_{PUCK}$(21)
		835	0.11	0.17	β(CCC)$_{PUCK}$(32), ω_{out}(CH) (27), ω(C$_{12}$=O$_{13}$) (18), Γ(CCCC)$_{R2}$ (11)
810 ms	811 vw	791	0.76	0.61	ω_{out}(CH) (40), β(CCC)$_{PUCK}$(22), ω(C$_{12}$=O$_{13}$) (10)
781 ms	790 vw	780	20.33	2.32	τ(O$\cdots$H$\cdots$O$\cdots$H) (27), τ(C$_{11}$O$_{14}$H$_{21}$$\cdots$O$_{25}$) (23), β (O$\cdots$H$\cdots$O) (15), Γ(C$_{11}O_{14}$) (15), τ(O$_{25}H_{26}$) (10)
		760	1.89	1.69	ω(C$_9$=O$_{15}$) (38), ω_{out}(CH) (17), Γ(CNC)$_{R3}$ (14),
751 vs	750 vw	750	0.81	1.28	ω(C$_9$=O$_{15}$) (45), Γ(CNC)$_{R3}$ (15), ω_{out}(CH) (5)
		737	2.44	3.77	β(CCC)$_{R1}$ (41), β(CC=O) (13), υ(CC)$_{R2}$ (10)
727 s	728 vw	731	5.25	3.94	ω_{out}(CH) (40), ω(C$_{12}$=O$_{13}$) (12), β(CCC)$_{PUCK}$(9), β(CCC)$_{R1}$ (6), υ(CC)$_{R2}$ (6)
671 s	674 vw	688	2.05	4.74	β(CCC)$_{R1}$ (48), β(C$_7$O$_{16}$) (8), β(NC=O) (8), υ(CC)$_{R2}$ (7)
655 s	656 vw	651	1.01	4.16	β(NC=O) (18), β(C$_{11}$O$_{14}$) (17), β(CCC)$_{PUCK}$(11), β(C$_7$O$_{16}$) (7), ω(C$_{12}$=O$_{13}$) (6), β(CCC)$_{R1}$ (5)
		605	0.47	4.92	β(CCC)$_{PUCK}$(17), υ(C-O) (15), ω_{out}(CH) (14), Γ(CCCC)$_{R1}$ (12), β(C$_7$O$_{16}$) (9)
593 ms	596 vw	578	13.70	1.72	τ(O$_{14}$H$_{21}$) (33), Γ(C$_{11}$O$_{14}$) (24), τ(O$\cdots$H$\cdots$O$\cdots$H) (12), υ(O$_{13}$$\cdots$H$_{21}$) (10), τ(O$_{25}H_{26}$) (10)
546 s	554 vw	543	0.53	7.46	υ(CC)$_{R2}$ (22), δ(CCC) $_{R1}$ (20), β(CCC)$_{ITR}$ (19), β(CCC)$_{R2}$ (11), β(CC=O) (10)
528 ms	534 w	537	0.65	13.14	υ(CN) (15), δ(C$_{11}$O$_{14}$) (13), τ(O$_{14}$H$_{21}$) (9), δ(CCC)$_{R1}$ (7), υ(CC)$_{R2}$ (7), τ(CNC)$_{R3}$ (6)
497 s	506 vw	519	1.58	1.04	Γ(CCCC)$_{R1}$ (29), δ(C$_7$O$_{16}$) (11), ω_{out}(CH) (8), ω(N$_{10}$H$_{23}$) (6)
		475	9.7	0.88	ω(N$_{10}$H$_{23}$) (29), τ(O$_{14}$H$_{21}$) (18), τ(C$_{11}$O$_{14}$) (14), υ(O$_{13}$$\cdots$H$_{21}$) (7), β(NC=O) (7)
454 vs	452 vw	453	2.04	0.58	Γ(CCCC)$_{R1}$ (64), ω_{out}(CH) (7)
424 ms	433 vw	446	12.96	1.41	τ(O$\cdots$H$\cdots$O$\cdots$H) (29), δ(O$\cdots$H) (14), Γ(CCCC)$_{R1}$ (12), β(NC=O) (9), τ(O$_{25}$H$_{26}$) (7)
419 ms	410 vw	418	1.80	1.51	τ(O$\cdots$H$\cdots$O$\cdots$H) (25), ω(N$_{10}$H$_{23}$) (14), τ(O$_{25}$H$_{26}$) (10), δ(O$\cdots$H) (9), β(NC=O) (8), υ(CN) (6)
		398	9.47	2.69	τ(C$_7$O$_{16}$) (49), δ(C$_7$O$_{16}$) (9), τ(O$_{14}$H$_{21}$) (7), ω(N$_{10}$H$_{23}$) (6), τ(C$_{11}$O$_{14}$) (6)
	388 vw	379	1.62	10.91	υ(CC)$_{R2}$ (23), δ(C$_7$O$_{16}$) (20), δ(CCC)$_{R1}$ (9), τ(CNC)$_{R3}$ (6), β(CCC)$_{ITR}$ (6)
	355 vw	375	2.61	3.55	δ(C$_{11}$O$_{14}$) (27), ω(N$_8$H$_{24}$) (18), δ(C$_7$O$_{16}$) (13), υ(O$\cdots$H) (10)
	336 vw	342	2.40	4.43	τ(CCCC)$_{R1}$ (17), υ(O$_{13}$$\cdots$H$_{21}$) (14), ω(N$_{10}H_{23}$) (13), ω(N$_8H_{24}$) (12), δ(C$_7O_{16}$) (7), υ(O$\cdots$H) (6)
	317 vw	321	2.67	2.90	υ(O$_{13}$$\cdots$H$_{21}$) (32), δ(C$_{11}O_{14}$) (14), β(CC=O) (14), υ(O$\cdots$H) (10), τ(CCCC)$_{R1}$ (8)
	301 vw	307	2.60	5.22	δ(C$_7$O$_{16}$) (37), υ(O$\cdots$H) (15), τ(C$_7$O$_{16}$) (14), δ(C$_{11}$O$_{14}$) (10)
		286	3.35	3.42	ω(N$_8$H$_{24}$) (39), τ(CCCC)$_{R1}$ (11), τ(C$_7$O$_{16}$) (9)
	256 vw	257	12.62	6.48	τ(O$_{25}$H$_{26}$) (67), δ(O$\cdots$H) (8)
	239 vw	244	0.36	1.14	β(CCC)$_{ITR}$ (16), υ(CC)$_{R2}$(15), δ(C$_7$O$_{16}$) (13), δ(CCC)$_{R1}$ (13), δ(C$_{11}$O$_{14}$) (7), τ(C$_7$O$_{16}$) (7)
	209 vw	199	1.55	9.16	τ(CNC)$_{R3}$ (25), δ(C$_{11}$O$_{14}$) (21), ω(C$_{12}$O$_{13}$) (12), τ(C$_7$O$_{16}$) (7), ω(N$_{10}$H$_{23}$) (7), δ(C$_7$O$_{16}$) (5)
	183w	167	0.54	0.42	υ(O$\cdots$H) (56), δ(C$_{11}$O$_{14}$) (11), υ(O$_{13}$$\cdots$H$_{21}$) (7), τ(O$_{25}H_{26}$) (6)
		145	0.07	18.88	ω(N$_8$H$_{24}$) (24), τ(CNC)$_{R3}$ (24), BTFLY$_{R1, R2}$ (10), δ(C$_7$O$_{16}$) (6), τ(CCCC)$_{R2}$ (6), ω(C$_{12}$O$_{13}$)

			(5)
136	1.49	1.55	$\upsilon(O\cdots H)$ (56), $\beta(CC=O)$ (8), $\tau(C_{11}O_{14})$ (8)
110	0.26	24.77	$\tau(CNC)_{R3}$ (32), $\omega(N_8H_{24})$ (24), $\tau(CCCC)_{R2}$ (19), $\tau(CCCC)_{R1}$ (6)
61	0.12	32.9	$\tau(CNC)_{R3}$ (51), $\omega(N_{10}H_{23})$ (19), $\tau(CCCC)_{R2}$ (12), $\omega(N_8H_{24})$ (11)
31	0.59	54.53	$\tau(CNC)_{R3}$ (38), $\omega(N_8H_{24})$ (29), $\tau(C_{11}O_{14})$ (7), $\tau(O_{25}H_{26})$ (6)
25	0.11	100	$\tau(CNC)_{R3}$ (39), $\omega(N_8H_{24})$ (30), $\tau(C_{11}O_{14})$ (9), $\tau(CCCC)_{R2}$ (6)

ν: stretching, γ: scissoring, ω: wagging, τ: torsion, Γ: twisting, β: in-plane bending, δ: out- of- plane bending, R_{br}: ring breathing, BTFLY: butterfly mode, ITR: inter-ring, R1: ring1-benzene ring, R2: ring2- fused cyclopentanone ring, R3: ring3- substituted urea moiety ring, in: in-plane, out: out-of-plane, s: symmetric, as: antisymmetric, vs: very strong, s: strong, ms: medium strong, vw: very weak, w: weak.

[a] Relative IR absorption intensities normalized with the highest peak absorption equal to 100.

[b] Relative Raman intensities normalized to 100.

Table 3: Calculated quantum chemical molecular orbital properties.

Parameters	B3LYP/cc-pVTZ
HOMO energy, E_{HOMO} (eV)	-7.1024
LUMO energy, E_{LUMO} (eV)	-2.4259
HOMO- LUMO energy gap, ΔE_{GAP} (eV)	4.6765
Ionisation potential, IP (eV)	7.1024
Electron affinity, EA (eV)	2.4259
Electronegativity, χ (eV)	4.7642
Chemical hardness, η (eV)	2.3383
Global softness, S (eV)$^{-1}$	0.2138
Chemical potential, μ (eV)	-4.7642
Electrophilicity index, ω (eV)	4.8534
Total energy change, ΔE_T (eV)	-0.5846
Overall energy balance, ΔE (eV)	-4.6765
SCF energy (eV)	-23757.6123

Table 4: Calculated electronic absorption spectral data of UNMH by TD-DFT/B3LYP/cc-pVTZ method.

Phase	Excited State, S	Electronic contributions (%)	Wavelength (nm)	Excitation energies (eV)	Oscillator Strengths, f	Assignment
Gas	S1(H→L)	79.1	346.57	3.5774	0.0039	n→π*
	S2(H-1 → L)	89.4	300.94	4.1199	0.0224	n→π*
	S3(H-2→L)	92.8	286.56	4.3267	0.0046	n→π*
Water	S1(H→L)	86.7	335.73	3.6930	0.0038	n→π*
	S2(H-1 → L)	90.9	292.10	4.2445	0.0404	n→π*
	S3(H-3→L)	73.2	268.04	4.6255	0.0281	n→π*

H:HOMO, L:LUMO.

TABLE CAPTIONS

Table 1: Optimized geometric parameters of UNMH.

Table 2: Experimental FT-IR, FT-Raman and theoretical wavenumbers in (cm^{-1}), IR and Raman intensities, vibrational assignments and PED contributions of UNMH by NCA based on SQM force field calculations.

Table 3: Calculated quantum chemical molecular orbital properties.

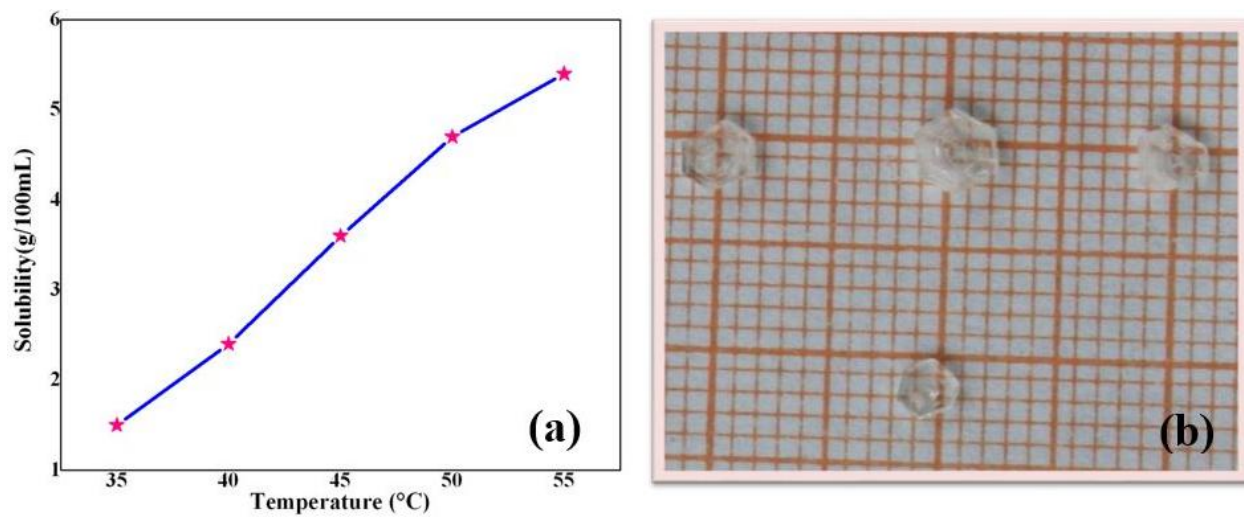**Table 4:** Calculated electronic absorption spectral data of UNMH by TD-DFT/B3LYP/cc-pVTZ method.

Figure

Fig. 1. (a) Solubility curve of UNMH. (b) Photograph of as-grown single crystals of UNMH.

Fig. 2. (a) Optimized structure of UNMH molecule. (b) and (c) two different views of the molecule.

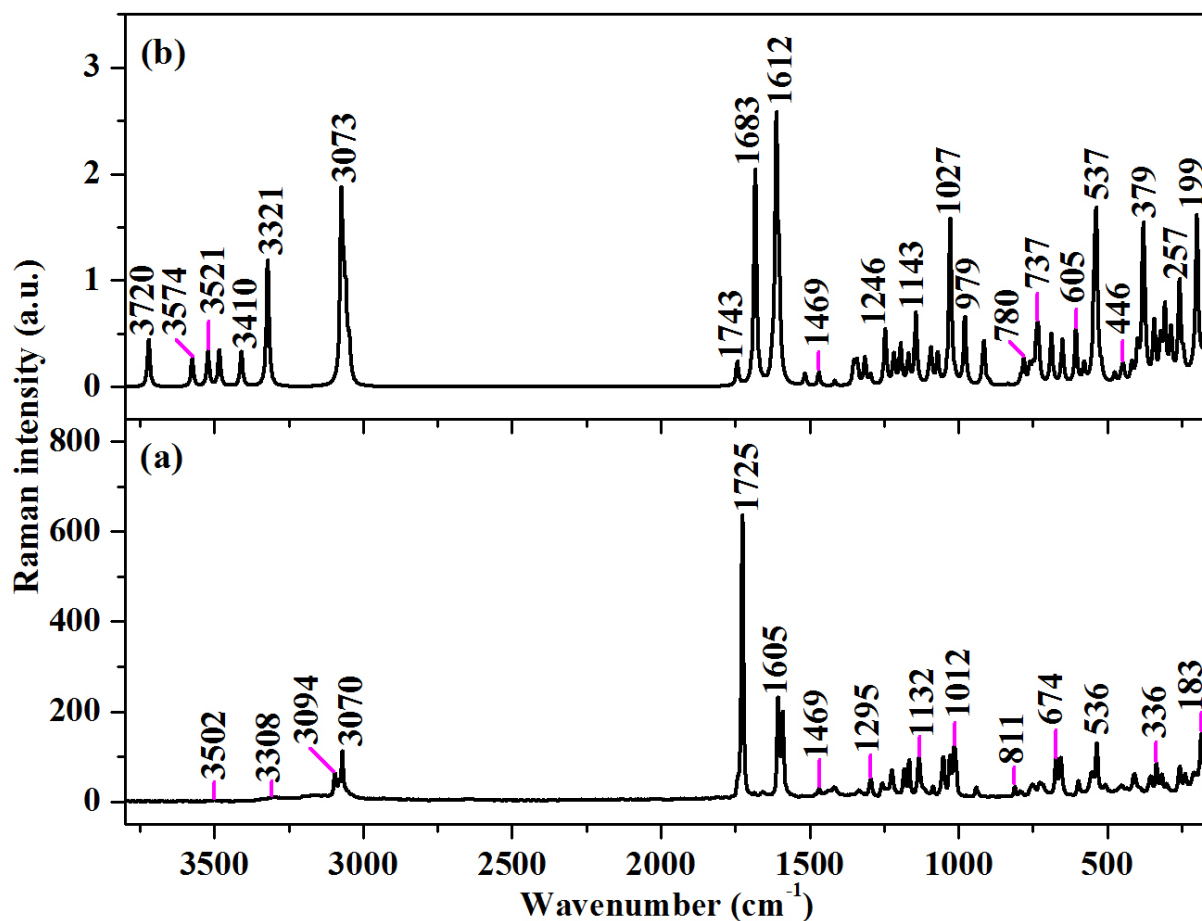**Fig. 3**. (a) Experimental FT-IR and (b) Simulated IR spectra of UNMH.

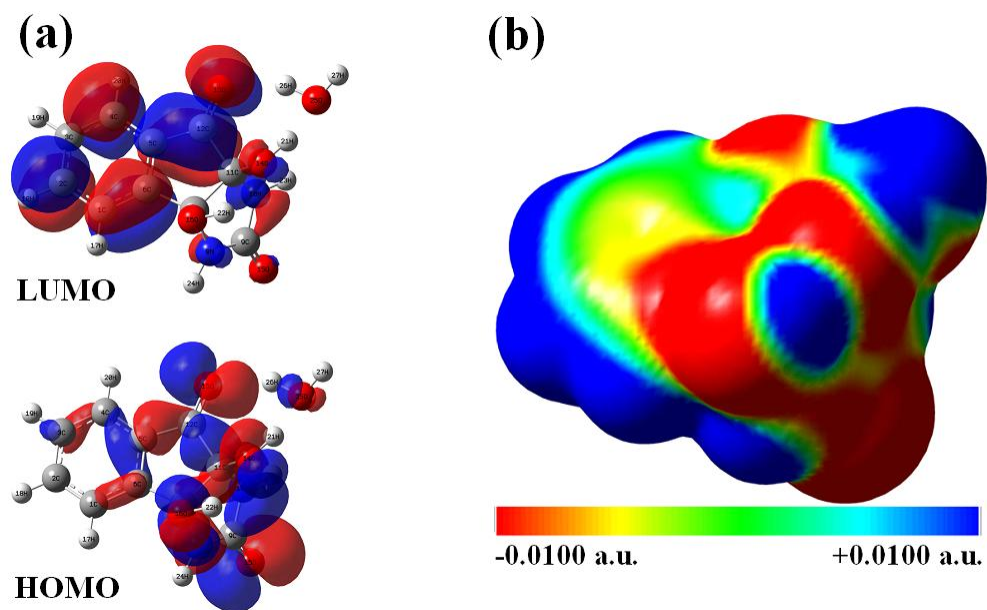**Fig. 4**. (a) Experimental FT-Raman and (b) Simulated Raman spectra of UNMH.

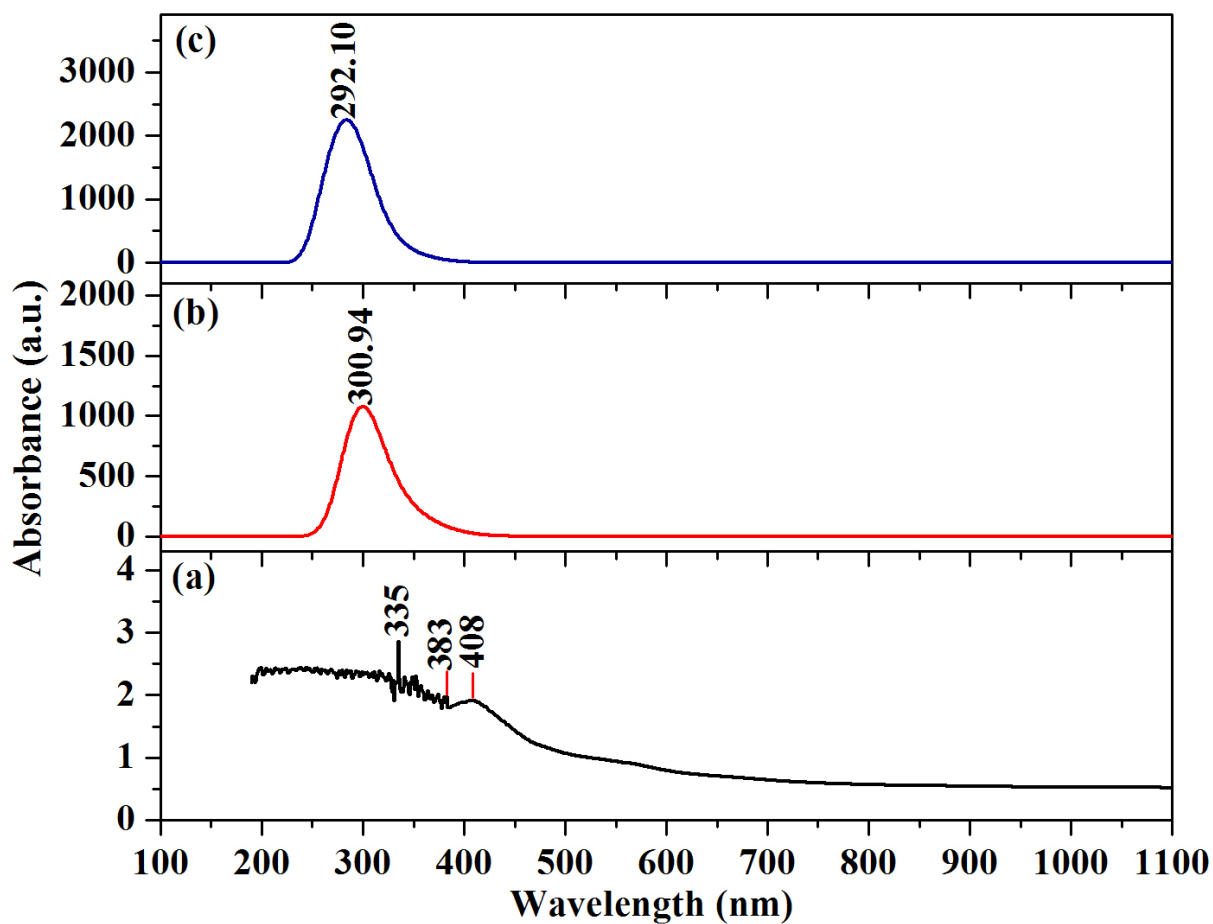**Fig. 5**. (a) Molecular orbitals. (b) Computed electrostatic potential on the molecular surface of UNMH.

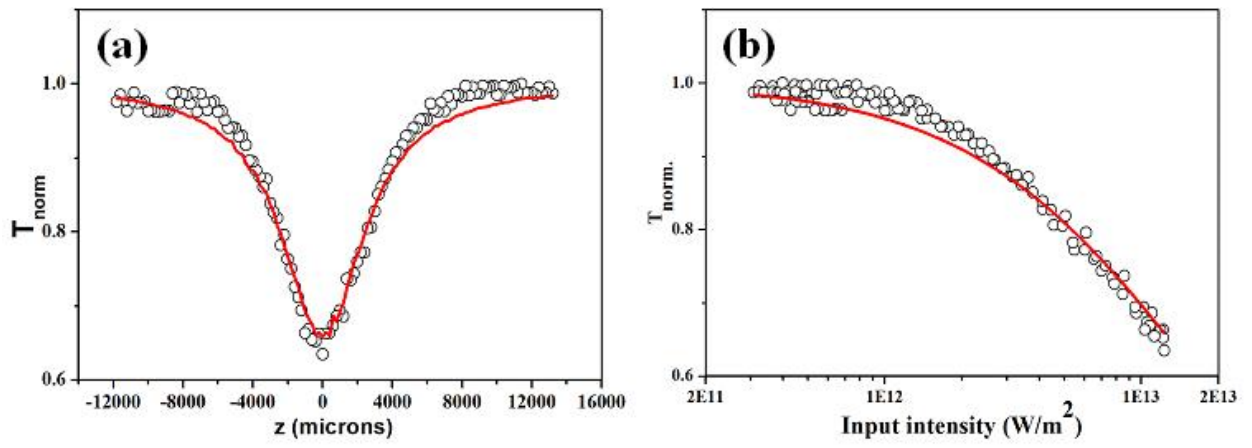**Fig. 6**. (a) Solid state UV-Vis-NIR and simulated UV-Vis-NIR spectra for (b) gas and (c) water phases of UNMH.

Fig. 7. (a) Open-aperture Z-scan curve. (b) Optical limiting curve of UNMH.

FIGURE CAPTIONS

Figure 1:(a) Solubility curve of UNMH. (b) Photograph of as-grown single crystals of

UNMH.

Figure 2:(a) Optimized structure of UNMH molecule. (b) and (c) two different views of
the molecule.
Figure 3:(a) Experimental FT-IR and (b) Simulated IR spectra of UNMH.

Figure 4:(a) Experimental FT-Raman and (b) Simulated Raman spectra of UNMH.

Figure 5:(a) Molecular orbitals. (b) Computed electrostatic potential on the molecular

surface of UNMH.

Figure 6:(a) Solid state UV-Vis-NIR and simulated UV-Vis-NIR spectra for (b) gas (c) water
phases of UNMH.
Figure 7: (a) Open-aperture Z-scan curve. (b) Optical limiting curve of UNMH.